When does turbulence spreading matter?

Rameswar Singh and P H Diamond
CASS, University of California San Diego,
*9500 Gilman Dr, La Jolla, CA 92093, USA**

(Dated: March 20, 2020)

Few, if any, of the many papers on turbulence spreading, address the key question of how turbulence spreading actually affect *profile structure*? Here we are using a reduced model to answer that question. Turbulence spreading is most relevant near regions where the profiles support a strong intensity gradient ∇I. One such case is at the edge of an L mode discharge, near a source of turbulence (i.e., either a localized source of edge turbulence or an influx of turbulence from the Scrape off Layer (SOL)). Another is in 'No Man's Land' (NML), which connects the pedestal to the stiff core in H mode. In the case of L mode, without an edge intensity source, the turbulence intensity profile is nearly flat and spreading has a weak effect. An edge localized source increases the edge ∇I, which then drives inward spreading. Invasion of turbulence from SOL to edge softens the edge pressure gradient. In H mode, the strong shear suppression of pedestal turbulence necessarily forces a sharp ∇I in NML. This sharp ∇I drives a significant flux of turbulence from the core to the pedestal, where it is ultimately dissipated by shearing. Counter-intuitively, results indicate that *spreading actually increases pedestal height and width and hence the energy content in H mode*. This suggests that models of pedestal structure should include NML turbulence spreading effects. The relation of avalanches to spreading is studied. Spreading weakly affects the avalanche distribution, but the spatiotemporal correlation of intensity increases with spreading.

* rsingh@ucsd.edu

I. INTRODUCTION

Turbulence spreading is a process of turbulence self-scattering by which locally excited turbulence spreads from place of excitation to other places. This is a phenomenon of inhomogeneous turbulence and is outside the realm of classic $K41$ paradigm. Naturally occurring turbulent systems and laboratory fluid dynamical systems such as pipe flows[1], plane Couette flow[2], turbulence in plasma and fusion devices exhibits inhomogeneous turbulence. In magnetized plasma turbulence, the fluctuation envelope is inhomogeneous on the mesoscales $l \subset (\rho_i, a)$ (ρ_i is ion larmor radius and a is minor radius) and so produces a flux of turbulence energy. Spreading is expected to impact transport and hence confinement. The radial spreading of turbulence has been widely observed in many global nonlinear simulations[3–7] and has been lately related to transport scaling modification[8]. This non-local phenomenon of turbulence spreading is frequently invoked as a mechanism for fast transients and other exotic phenomena, like the breakdown of gyro-Bohm transport scaling[8–10], and the breakdown of Ficks law[11]. Turbulence penetrates internal transport barrier and limits its performance[12]. Turbulence spreading through a magnetic island has been observed both in gyrokinetic simulations[13, 14] and experiments[15, 16]. Other indirect evidence of turbulence spreading in action include observation of anomalous transport in the core of NSTX[17], observation of non-zero fluctuations and anomalous transport in the the linearly stable zone of a $JT-60U$ reverse shear discharge[18]. Indirect evidence of turbulence spreading is seen just after transport barrier formation or its collapse. Fluctuation levels in the core drops in a short time scale (much shorter than transport time scale) after H mode transition in DIII-D tokamak[19]. In the TJ-2 stellerator, the density fluctuations at the inner radii increase on the same time scale as the time scale of collapse of the edge radial electric field shear during H-L back transition[20]. In the inner core ($\rho < 0.2$), even in cases without apparent MHD (e.g. when $q > 1$), the measured temperature and density gradients tend to flatten and local simulations tend to predict spurious stability. The turbulence spreading from outer core to the inner core can help sustain the lower gradients in this central region. Finally, there is the transport short-fall problem: Some earlier local non-linear simulations[21, 22] considerably underpredicted the turbulence and transport level in No Man's Land (NML), as compared to experimental measurements. NML is the interface region connecting the pedestal top to the stiff core (see figure(2)). However this underprediction was later addressed by changing

the turbulence drive (i.e., temperature gradient) in the local simulations by a few percent. This small change lies within the experimental error bars[23, 24]. But local simulations do not treat the turbulence spreading effect correctly. While local multi-scale simulation can resolve some of the shortfall question, there is still room for modelling including spreading effects and for further studies with global, flux driven simulations. These observations can not be reconciled within the framework of local turbulence and transport. These are some situations where turbulence spreading may come to rescue.

Turbulence spreading is often modelled theoretically as propagating intensity front solutions of the Fisher-KPP[25, 26] nonlinear reaction-diffusion equation[10]. The reaction term consists of sum of linear growth and nonlinear damping (usually quadratic) in intensity. The intensity diffusion term is also nonlinear, with diffusivity proportional to intensity itself i.e. $\propto I$. A profile of linear growth rate is prescribed to study spreading of an initial slug of turbulence in *frozen* background profiles. This approach has, no doubt, lead to some understanding of turbulence spreading from unstable to stable zone and sheds some light on the origin of breakdown of gyro-Bohm transport scaling[10]. Spreading from an unstable to a stable zone leads to reduction of intensity in the unstable zone and introduces an additional dependence on $\rho_\star = \rho_i/a$ to the turbulence intensity, which is otherwise determined by local physics. This leads to a deviation of transport scaling from gyro-Bohm scaling. However, physical plasma systems are flux driven which means the total flux (turbulent + classical flux) must balance the input flux profile in steady state. This constraint forces profiles to evolve with intensity spreading. Hence we relax the frozen profile assumption, to study the effect of spreading on steady state profiles.

From a fusion point of view, anything affecting confinement is of immediate interest. So we ask the following questions.

1. How does turbulence spreading influence profiles?
2. In the cases where it does, what are the distinguishing features?

Before proceeding with a description of the model used and the results obtained in this paper, we compare and contrast our work with previous works. Most of the previous theoretical and simulation studies on turbulence spreading simply focused on spreading of a slug of turbulence which ignored its effect on profile evolution. These include the various works illustrated below, and contrasted with our work in table(I). The works of Garbet *et*

al[27], Naulin *et al*[28] and Wang *et al*[29] considered the pressure, density and temperatures equations respectively self consistently, and studied transient evolution of a pulse of turbulence. They ignored the question of how spreading affects the steady sate profiles, which directly map to confinement. This pinpoints why our study of spreading effect on profiles is important. Pulse propagation is important if one is specifically interested in fast transient nonlinear response. Steady state profiles are at least of importance from fusion perspective. This is why this paper is distinct from the previous works.

Models	What is studied?	Relevance
1-field (I)[10][30]	Space-time evolution of a pulse of turbulence in *frozen* background	*Fast transients* on time scales shorter than transport time
2-fields (I &P)[27]	Space-time evolution of a pulse of turbulence in *frozen* background	*Fast transients* on time scales shorter than transport
2 fields (I & n)[28]	Space-time evolution of a pulse of$I$ & n	Fast transient response on time scales shorter than the transport time
2 fields (I and T)[29]	Intensity pulse speed with heat flux	Fast transient response on time scales shorter than the transport time
Delta-f gyrokinetic PIC simulation with gKPSP[31]	Magnetic shear effect on spreading in frozen background	Demonstrated that spreading is most effective at intermediate values of magnetic shear (~ 0.5)
GYRO simulations[32]	Spreading in piecewise-flat profiles.	Illustrated breaking of gyro-Bohm scaling due to spreading
GTS simulations[33]	Spreading through an externally imposed $E \times B$ shear well.	Demonstrated blocking of spreading through shear layer
GTC simulations[34]	Spreading through q_{min} in frozen background	Demonstrated that steady sate turbulence fills the whole volume without any gap at the q_{min} location
Delta-f gyrokinetic PIC simulation[8]	Steady state profiles of turbulence intensity at different $\rho_\star$ in *frozen* background	Demonstrates turbulence intensity in linearly stable zone
L mode: 2 fields (I & P); H mode: 3 fields (I, P & n)(this work)	Effect of spreading on steady state profiles	*Profile structure, confinement*

Table I. Comparing and contrasting our work with others. I, P, and n represent turbulence intensity, pressure and density respectively.

Turbulence spreading matters whenever there is a strong intensity gradient. In L mode, the turbulence intensity monotonically increases radially outward. This could be due to strong resistive edge turbulence or due to the invasion of turbulence from scrape off layer (SOL). Hence spreading is expected to have some effect on profiles. In this paper, effects of turbulence spreading on L mode profiles are studied in a simple 2-field model consisting of intensity(I) and pressure(P) evolution equations. The strong edge turbulence in L mode is modelled by using an additional edge localized source in the intensity equation. Turbulence invasion from SOL is modeled using a finite in-flux boundary condition at the edge. Either way, enhanced edge turbulence softens the edge pressure gradient and degrades confinement. The inward turbulence spreading then reduces the edge intensity and increases the core intensity. This causes steepening of edge pressure gradient. However this effect is negligible, without an edge localized source or turbulence invasion from SOL, due to mild intensity profile gradient near the edge. This is schematized in figure(1).

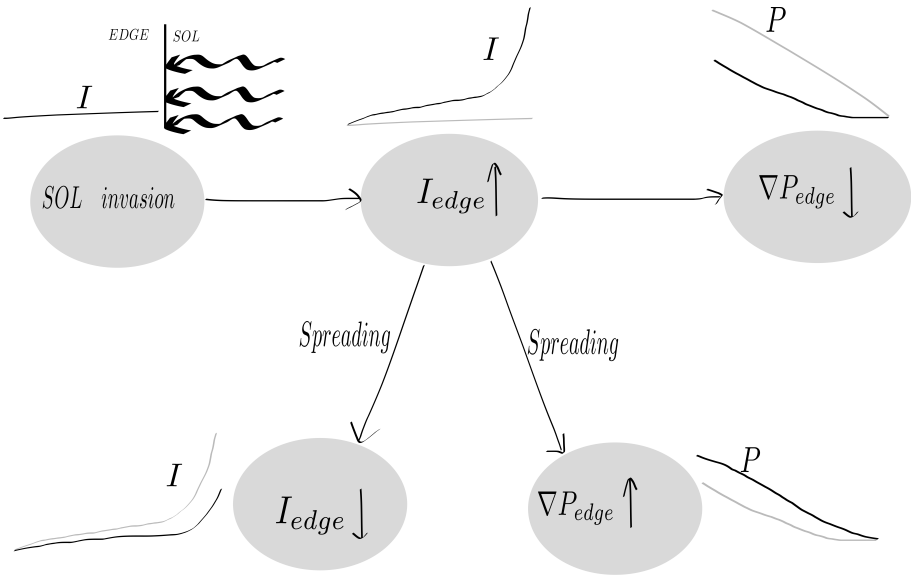

Figure 1. Schematic of spreading effect with edge source of intensity due to invasion from SOL or localized edge source. I and P represent turbulence intensity and pressure respectively.

In H mode, we argue that turbulence spreading in No Man's Land (NML) has a significant effect on pedestal height and width, issues of great pragmatic interest. Understanding the physics mechanisms determining barrier height and width are of utmost importance because the latter impact global confinement. Generally, bigger barrier height and width are better for confinement. Edge transport barriers appear as a result of the suppression of edge turbulence by enhanced $E \times B$ shear due to bifurcation of radial electric field at higher input power[35–37]. H mode pedestal height and width are usually controlled by the input heat, particle and momentum fluxes. However the width and height of the pedestal do not continue to increase without bound. The stable limiting size of the pedestal is thought to be set by peeling-ballooning stability[38]. In this conventional wisdom, the role of turbulence spreading is ignored.

Turbulence spreading can play a significant role in determining the radial profile of turbulence intensity and hence sets the extent of the region of turbulence suppression. Turbulence spreading is most active in regions of strong turbulence intensity gradient. So NML near the pedestal top in H mode is a place where turbulence spreading effects are very strong. This is schematized in figure(2).

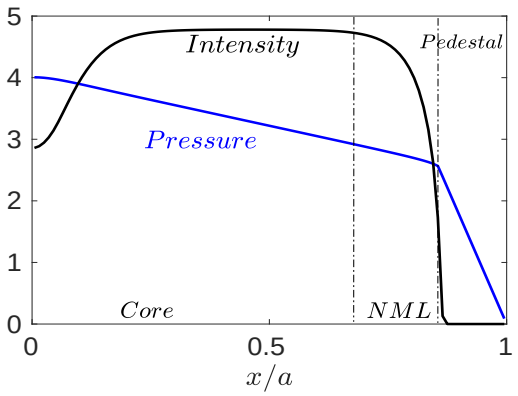

Figure 2. Turbulence intensity and pressure profile at weak spreading. Also rough partitions of core, pedestal, and NML are shown. Clearly intensity gradient is strong in NML.

In this paper effects of turbulence spreading on H mode pedestal size are studied

in a 3-field model which self-consistently evolves density(n), pressure(P) and turbulence intensity(I). Pressure and density fluxes are treated as bi-stable due to $E \times B$ shear suppression of turbulent diffusivity and a constant neoclassical diffusivity. Turbulence intensity is excited by critical pressure gradient with $E \times B$ shear reduction of the linear growth rate and saturated by non linear damping. Turbulence spreads via nonlinear diffusion of intensity. The effect of spreading is studied by varying the effective Prandtl number- defined as the ratio of the turbulent intensity diffusion coefficient to the turbulent heat diffusion coefficient. We find that turbulence spreading in fact elevates the pedestal (maintaining the pedestal pressure gradient) by reducing turbulence intensity in NML. Indeed, turbulent intensity in NML is strongest when spreading is weakest, as shown in the schematic in figure(2). With increasing Prandtl number, the turbulence intensity in NML decreases and pedestal height and width increase. We also see that turbulence penetrates the pedestal and that depth of penetration increases with Prandtl number. Hence turbulence spreading plays a positive role in confinement improvement in H mode. In contrast, spreading has a weak effect on L mode confinement, though it is often invoked to explain the breakdown of gyro-Bohm scaling.

Finally, we must mention that our approach is somewhat at best semi-quantitative. No numerical simulation has identified effect of spreading on profiles. There is no unique control parameter for spreading in gyrokinetic simulations or in experiments. No data from experiments and simulations exist that can be used for quantitative comparison with our results on spreading effect on plasma profiles at steady state. This supports our semi-quantitative approach which helps in understanding of the role of turbulence spreading on profile formation.

Nevertheless, our results suggest that predictive models of pedestal structure must address NML turbulence and spreading effects. Core turbulence simulations use pedestal parameters from pedestal models, e.g. EPED, as a boundary condition. But the pedestal structure models do not have turbulence spreading effects. So, accuracy of such core turbulence simulations may be compromised.

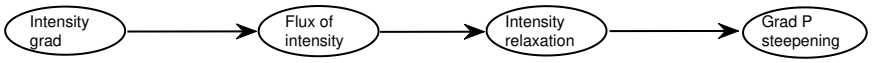

Figure 3. Schematic of spreading effect on profile

The schematic shown in figure(3) summarizes the effect of spreading on profile. Spreading leads to local reduction of turbulence and steepening of pressure gradient. This is true in general and irrespective of confinement regime type. However the spreading effect on profile is more significant in H mode (compared to L mode) due to strong intensity gradient at NML.

The rest of the paper is organized at follows. In Section(II), a self-consistent 3-field model for coupled evolution of turbulence intensity, pressure and density profiles is described. This model is used to study turbulence spreading effect on profiles. This is then, reduced to a 2-field model to study spreading effects in L mode in Section(III). The spreading effects on H mode profiles are described in Section(IV). Finally the paper is concluded with a discussion in Section(V).

II. COUPLING TURBULENCE SPREADING TO PROFILES

Conventionally, turbulence spreading is treated as a Fisher-KPP type 1d reaction diffusion equation. This is in the spirit of a $K-\varepsilon$ model[39] for the turbulence intensity field used in subgrid-scale modeling, where K is kinetic energy and ε is dissipation. The turbulence intensity $I\left(=\left|\frac{e\delta\phi}{T}\right|^2\right)$ is evolved as

$$\frac{\partial I}{\partial t}=\chi\left[\mu I-\gamma_{NL}I^2\right]+\sigma\frac{\partial}{\partial x}I\frac{\partial I}{\partial x} \tag{1}$$

where the first term on the right hand side represents local linear turbulence drive, with μ the growth or damping rate. The second term results in nonlinear saturation of the intensity at the mixing length level $I=\mu/\gamma_{NL}$, when $\mu>0$. The nonlinear damping γ_{NL} is due to local mode-mode coupling. The third and final term is the nonlinear diffusion of the

turbulence intensity due to mode-mode coupling, which results in spatial scattering. The nonlinear turbulent diffusion term arises naturally when nonlinear coupling in k-space and nonlinear scattering in x-space are treated on equal footing using a multi-scale closure of $E \times B$ non-linearity, which treats both mode k and envelope scales, *i.e.* $\vec{\nabla} \to i\vec{k} + \partial_x$[40].

$$\sum_{k'} \left(\vec{k} \cdot \vec{k}' \times \vec{z}\right)^2 I_{k'} R(\vec{k}, \vec{k}') I_k \to -\frac{\partial}{\partial x} D_x(I_k) \frac{\partial I_k}{\partial x} + k_\perp^2 D_k I_k \tag{2}$$

where $R(\vec{k}, \vec{k}')$ is a response function which determines the correlation time, $D_x = \sum_{k'} R(\vec{k}, \vec{k}') \left|\delta V_{E,k'}\right|^2$, and $D_k = \sum_{k'} \left(\vec{k} \cdot \vec{k}' \times \vec{z}\right)^2 R(\vec{k}, \vec{k}') \left|\delta V_{E,k'}\right|^2$. The first term is the (radial) nonlinear diffusion, and the second represents local nonlinear transfer. We note that other forms of diffusivity are possible, but the choice $D(I) = \sigma I$ is usually made as this correspond to weak turbulence closure[41]. As shown by Gurcan *et al*[30], equation(1) can be derived from a Fokker-Planck type analysis of the intensity field evolution in space, assuming intensity random walks due to turbulence scattering with a step size of the turbulence correlation length and time step equal to the correlation time. This equation can also be derived by application of quasi-linear theory to the wave kinetic equation.

Some of the drawbacks of the Fisher model are the following. The Fisher model equation(1) supports travelling front solutions connecting turbulent and laminar fixed points only in the linearly unstable region. Moreover, this model predicts very weak penetration of turbulence into linearly stable regions, with characteristic depth of penetration $\lambda = \sqrt{\frac{\sigma}{\gamma_{NL}}}$[30]. This can not explain the large fluctuation levels observed in linearly stable zones like internal transport barrier in JT-60U[42]. Finally the biggest drawback is that the Fisher model ignores self-consistent coupling to profile evolution.

A recent advance[43] on this type of the model was developed. This is based on bi-stable and sub-critical turbulence, similar to that for Poiseuille and plane Couette flows[44] and pipe flow transition to turbulence[1, 45]. This model seems to overcome the first two drawbacks above. The bi-stable sub-critical model reads

$$\frac{\partial I}{\partial t} = \chi \left[\mu I + 2\beta I^2 - I^3\right] + \sigma \frac{\partial}{\partial x} I \frac{\partial I}{\partial x} \tag{3}$$

The following observations support the choice of of the above phenomenological model for sub-critical turbulence spreading in magnetized fusion plasma. Inagaki *et al.*[46] have demonstrated global hysteresis between the turbulence intensity and the local temperature gradient

in the Large Helical Device L mode plasma. This hysteresis itself implies a memory in the turbulence and suggests the possibility of a bi-stable relationship between the intensity and the local gradient. We note that this hysteresis can also be explained by a mismatch in the assumed heat deposition profiles during the heat modulation[47]. From theory and simulation, the 3D Hasegawa-Wakatani system is known to be sub-critical in the presence of magnetic shear, due to a nonlinear streaming instability[48–50]. Collisional electrostatic drift-wave turbulence in a sheared slab described by cold ion Braginskii equations is shown to be self-sustained when initialized at nonlinear amplitude[51, 52]. Guo and Diamond[53] argued that the turbulence exhibits bi-stability in the vicinity of temperature corrugations in the $E \times B$ staircase, a self- organized structure of quasi-periodic shear flow layers. These corrugations arise due to inhomogeneous turbulent mixing and drive ion-temperature-gradient-driven (ITG) turbulence locally, which can result in further roughening of the temperature profile and thus nonlinear turbulence drive. A sufficiently strong ambient perpendicular shear flow can also cause the turbulence to be sub-critical —this effect has been observed in gyrokinetic simulations[54, 55]. Finally, we note that phase-space structures such as holes and granulations, which can interact with drift waves[56], are known to drive nonlinear instabilities[57]. Bi-stable sub-critical turbulence makes for stronger penetration of the stable zone[43]. The bi-stable regime supports traveling turbulence front solutions, with characteristic length scales which are qualitatively similar to those of the Fisher model yet penetrate the linearly stable or marginal region. An new propagating wave solution is possible in the linearly stable region with reduced amplitude and speed.

Hence we make a two pronged improvement to the Fisher model. First, the reaction term in Fisher equation is generalized to treat sub-critical bi-stable turbulence. Second, the intensity equation is self-consistently coupled to the pressure and density profile evolution equations. The linear growth rate of intensity is related to the local pressure gradient, and the turbulent heat flux in pressure equation and particle flux in the density equation is proportional to local intensity. We consider following 3-field continuum model consisting of turbulence intensity I, pressure P and density n

$$\frac{\partial I}{\partial t} = f(I, P, n) + \sigma \frac{\partial}{\partial x} I \frac{\partial I}{\partial x} \tag{4}$$

where the first term on the right hand side is the reaction term which consist of turbulence growth and damping and is a function of I, P and n. σ is spreading coefficient. Note that the nonlinear diffusion term do not produce any source term in the intensity equation(4). This is explained in the Appendix(A).

$$\frac{\partial P}{\partial t} = \frac{\partial}{\partial x}\left(\frac{\alpha_p I}{1+\epsilon V_E'^2} + D_{cp}\right)\frac{\partial P}{\partial x} + S_p \tag{5}$$

and

$$\frac{\partial n}{\partial t} = \frac{\partial}{\partial x}\left(\frac{\alpha_n I}{1+\epsilon V_E'^2} + D_{cn}\right)\frac{\partial n}{\partial x} + S_n \tag{6}$$

where a bi-stable form of flux due to shear suppression is used. α_p and α_n are turbulent pressure and density diffusivity coefficients respectively. D_{cp} and D_{cn} are neoclassical pressure and density diffusivities. The $E \times B$ velocity shear V_E' is obtained from the radial force balance, assuming no poloidal and toroidal flows $V_E' = -\frac{1}{eBn^2}\frac{dp}{dx}\frac{dn}{dx}$. Note that the contribution of pressure curvature is also ignored. The pressure source is chosen as localized at the core and density source is localized at the edge, with the functional forms $S_p = S_{0p}e^{-w_p x^2}$ and $S_n = S_{0n}e^{-(x-x_0)^2}$ respectively. Above model is solved numerically for the boundary conditions $\frac{\partial I}{\partial x}(x=0) = \frac{\partial I}{\partial x}(x=a) = 0$, $\frac{\partial n}{\partial x}(x=0) = \frac{\partial P}{\partial x}(x=0) = 0$, $n(x=a) = 0.01$ and $P(x=a) = 0$. Here a represents minor radius of tokamak. Note that the turbulence intensity at the edge in L mode is significantly enhanced, compared to the core. This can be modeled either by adding a localized source of intensity or by setting up a finite intensity flux boundary condition at the edge.

III. SPREADING EFFECT IN L MODE

A. Model for L mode studies

Note that in L mode, transport bifurcations do not occur. So the $E \times B$ shearing effect can be ignored in the equations. In such as a situation the neoclassical diffusion terms can also be ignored as turbulent diffusion dominates. Also density equation is needed to localize $E \times B$ shear towards the edge. Since shearing feedback can be ignored in L mode, we consider the following subset of equations consisting of intensity and pressure only. Retaining the bistable subcritical reaction term $f = \chi\left[\mu I + 2\beta I^2 - \delta I^3\right]$ the intensity equation reads as:

$$\frac{\partial I}{\partial t} = \chi\left[\mu I + 2\beta I^2 - \delta I^3\right] + \sigma\frac{\partial}{\partial x}I\frac{\partial I}{\partial x} + \delta(x-a)\frac{I_0}{\tau} \tag{7}$$

where the first term on the right hand side represents local linear turbulence drive, with growth rate $\mu = \left(\left(\frac{\partial P}{\partial x}\right)^2 - \mu_c^2\right)$, μ_c is the critical pressure gradient. The growth rate is positive only when the pressure gradient exceeds the critical gradient. χ is total growth rate. β measures the strength of nonlinear growth. $\beta > 0$ yields sub-critical turbulence, $\beta = 0$ yields supercritical turbulence. I_0 is an edge localized source of turbulence intensity added to model additional edge turbulence as seen in experiments. The pressure evolution equation is reduced to

$$\frac{\partial P}{\partial t} = \frac{\partial}{\partial x}\alpha_p I\frac{\partial P}{\partial x} + S_p(x), \qquad S_p = S_{p0}e^{-w_p x^2} \tag{8}$$

where α is turbulent pressure diffusion coefficient. Above model is solved numerically for the boundary conditions $\frac{\partial I}{\partial x}(x=0) = \frac{\partial I}{\partial x}(x=a) = 0$, $\frac{\partial P}{\partial x}(x=0) = 0$, $P(a) = 0$. Enhanced turbulence intensity at the edge may also result from the turbulence invasion from the scrape off layer (SOL). This can be modeled by setting $I_0 = 0$ and setting up a finite intensity flux boundary condition $\frac{\partial I}{\partial x}(x=a) \neq 0$ at edge. Noise is added to the pressure source to excite avalanches. Noise in pressure source is not unrealistic, as all thermal and particle sources are in practice noisy. Note that this reduced model for L mode also has fewer free parameters than the full model does. We introduce following normalizations for the numerical calculations. Space and time is normalized as $x \to \hat{x} = x/a$, $t \to \hat{t} = t\rho_\star^2 c_i/a$, where $\rho_\star = \frac{\rho}{a}$. Pressure is normalized by reference value $P_0[= 1 \times 10^{19} KeVm^{-3}]$: $P \to \hat{P} = P/P_0$. Turbulent diffusivities generally $\propto \chi_{GB}\frac{I}{\rho_\star^2}$. Hence this normalization leads to $\sigma \to \hat{\sigma} = \sigma/\chi_{GB}$, $\alpha_P \to \hat{\alpha}_P = \alpha_P/\chi_{GB}$. The intensity is normalized as $I \to \hat{I} = I/\rho_\star^2$. Also effective growth rate as $\chi \to \hat{\chi} = \chi a/c_i\rho_\star^2$ and the dimensionless parameters as $\beta \to \hat{\beta} = \beta\rho_\star^2$, $\delta \to \hat{\delta} = \delta\rho_\star^4$. The source is normalized as $S_p \to \hat{S}_p = aS_n/n_0 c_i\rho_\star^2$. The normalized equations look same as the original equations with "hatted" variables.

B. Results for L mode

Defining Prandtl number as $Pr = \frac{\hat{\sigma}}{\hat{\alpha}}$, scans of steady state profiles with respect to Pr with different combinations of $\hat{\sigma}$ and $\hat{\alpha}$, $\hat{\beta}$ and $I_0/\hat{\tau}$ were made. We discuss the results of

Pr scan below.

For fixed value of Pr resulting from different combinations of $\hat{\sigma}$ and $\hat{\alpha}$, the profiles of I and P are different. This means that the system of equations can not be re-scaled in terms of Pr. The net turbulence energy $\int dxI$, increases and total confinement $\int dxP$ degrades, with increasing $\hat{\beta}$. As a result, a supercritical pressure profile at low $\hat{\beta}$ may become a sub-critical profile at high $\hat{\beta}$, for fixed input power. Variations in $\hat{\alpha}$ cause more pronounced effect in pressure and intensity profiles. Decreasing $\hat{\alpha}$ increases both confinement and turbulence intensity. Pressure gradient steepens and edge intensity rises. This result is due to lack of self-consistent $E \times B$ shear suppression of turbulence in our simple L mode model.

1. ***Spreading in presence of an edge localized source:*** In L mode plasma, turbulence intensity monotonically rises with radius, making the edge turbulence intensity higher than that in the core. Our simple model, without an edge source of intensity either due to local effect or due to incoming flux of turbulence from SOL, produces an almost flat intensity profile at the edge. Hence to model an increasing profile of intensity a localized edge source of intensity is used in the intensity equation. Increasing the edge localized source increases the edge turbulence intensity, which softens the edge pressure gradient with overall confinement degradation. Edge intensity is affected more than the pressure gradient. Now increasing $\hat{\sigma}$ in general reduces edge turbulence intensity and enhances core turbulence intensity. As a result the edge pressure gradient steepens and core confinement degrades. However this effect is more noticeable in the presence of edge intensity source which makes edge intensity gradient strong. This is evident in figure(4). Otherwise, the effect of spreading on the pressure profile is very weak. Steady state profiles are independent of the form of the initial profiles (not shown here).

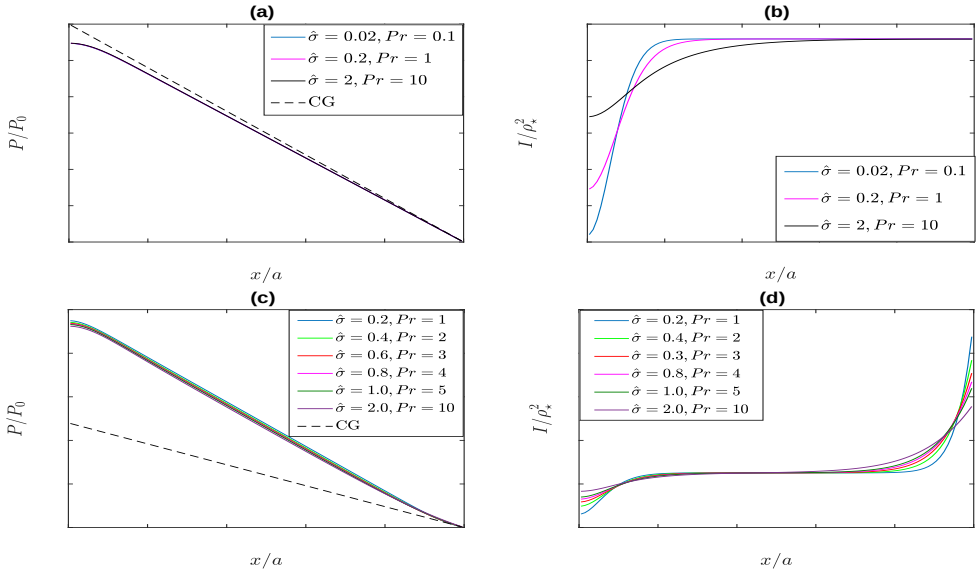

Figure 4. $\hat{\sigma}$ scans of pressure (a) and intensity (b) profiles at $\hat{\chi} = 20$, $\hat{\beta} = 2.5$, $\hat{\alpha} = 0.2$, $\mu_c = 1.2$, $\hat{\delta} = 1$, $\hat{S}_p = 13e^{-100\hat{x}^2}$ without edge source $I_0/\hat{\tau} = 0$. $\hat{\sigma}$ scans of pressure (c) and intensity (d) profiles at $\hat{\chi} = 20$, $\hat{\beta} = 0$, $\hat{\alpha} = 0.2$, $\mu_c = 1.2$, $\hat{S}_p = 13e^{-100\hat{x}^2}$ with edge source $I_0/\hat{\tau} = 10^4$. Initial profiles $I(x) = 0.1e^{-100(\hat{x}-1)^2}$ and $\hat{P}(x) = 0.4(1-\hat{x}^2)$. The dashed line labeled CG is the critical gradient profile.

2. ***Spreading effect with SOL turbulence invasion:*** A similar qualitative effect is seen without an edge localized source but with turbulence invasion from the SOL. This is modeled as a finite influx boundary condition at the edge. A finite influx at the edge produces an intensity profile monotonically increasing in radius. Turbulence spreading effects on the pressure profile are again more pronounced, due to strong edge intensity gradient. SOL turbulence invasion increases edge turbulence intensity, which softens the edge pressure gradient leading to over-all confinement degradation. Softening of the edge pressure gradient depends on edge intensity and follows a linear relation on a log-log scale. This relation is independent of whether turbulence is produced locally or is result of invasion from SOL, i.e., see fig(5).

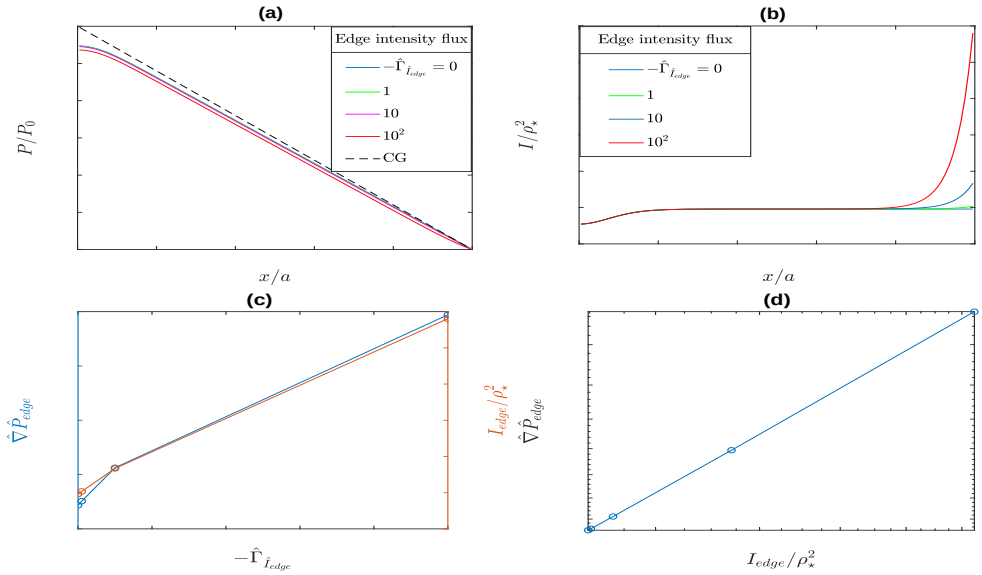

Figure 5. Pressure (a) and intensity (b) profiles with normalized edge intensity flux $\hat{\Gamma}_{\hat{I}} = -\hat{\sigma}\hat{I}\frac{\partial \hat{I}}{\partial \hat{x}}$. The physical intensity flux Γ_I and the normalized intensity flux $\hat{\Gamma}_{\hat{I}}$ are related as $\Gamma_I = c_i\rho_\star^4\hat{\Gamma}_{\hat{I}}$. (c) Edge intensity flux scan of edge intensity and edge pressure gradient at $Pr = \frac{\hat{\sigma}}{\hat{\alpha}} = 1$. (d) Edge intensity and edge pressure gradient relation. Parameters $\hat{\chi} = 20$, $\hat{\beta} = 2.5$, $\hat{\alpha} = 0.2$, $\hat{\sigma} = 0.1$, $\mu_c = 1.2$, $\hat{\delta} = 1$, $\hat{S}_p = 13e^{-100\hat{x}^2}$. Initial profiles same as in figure(4).

3. ***Interaction of spreading and avalanching:*** Avalanches are excited by a white noise in the pressure source. Avalanches are quantified by frequency spectra of intensity fluctuation and fluxes obtained from respective time histories. The results capture typical features of frequency spectra as commonly seen in gyro-kinetic and sand-pile simulations. The frequency spectrum has three distinct regions. In low frequency region the power spectrum is almost flat and scales as ω^0. In high frequency region the power spectrum scales as $\omega^{-\alpha}$, where $\alpha > 1$ and is different for intensity and heat flux spectra. For the intensity spectrum $\alpha = 2$ and for heat flux spectrum $\alpha = 2.5$. The intermediate frequency region of the spectra scales as ω^{-1}. These three spectral regions have also been identified in sand-pile models[58, 59], fluid simulations of resistive pressure gradient driven turbulence[60], dissipative trapped electron mode turbulence[61] and full-f global flux driven

gyrokinetic simulations[62]. The effect of sub-critical parameter dependence and spreading on the avalanche distribution are studied. We notice that noise promotes spreading at early times. The frequency spectra of intensity and fluxes are weakly affected by $\hat{\beta}$, as shown in fig(6). Turbulence spreading weakly affects the avalanche distribution as seen from the Prandtl number scan of frequency spectra of fluctuations and fluxes, see figure(7). Both correlation time and and correlation length of the intensity fluctuations increases with Prandtl number as can be seen from 2D space-time auto-correlation function shown in figure(8). We also observe that inward and outward velocities are not symmetric and the in-out velocity asymmetry increases with Pr.

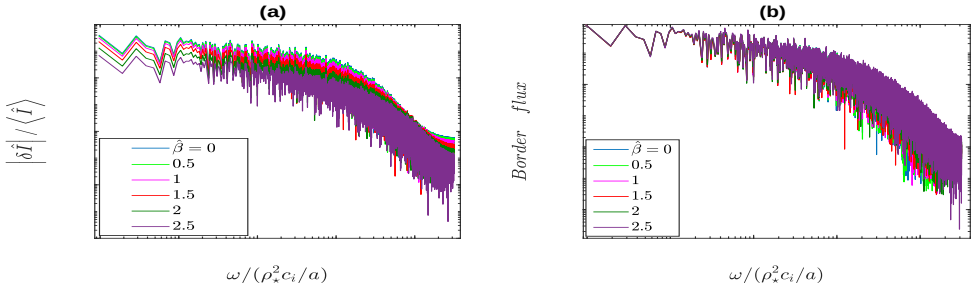

Figure 6. Frequency spectra of normalized intensity $|\delta I|/\langle I\rangle$ (a) and edge heat flux (b) with $\hat{\beta}$ at $Pr = 1$. The downward shift of the frequency spectra is because the time averaged intensity $\langle I\rangle$ increases with $\hat{\beta}$.

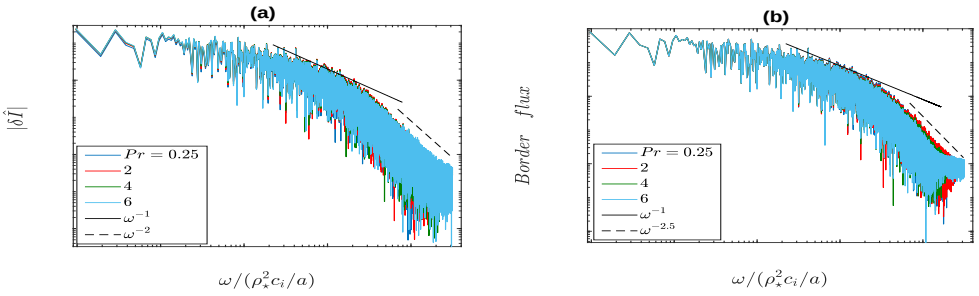

Figure 7. Frequency spectra of intensity (a) and edge heat flux (b) with Pr.

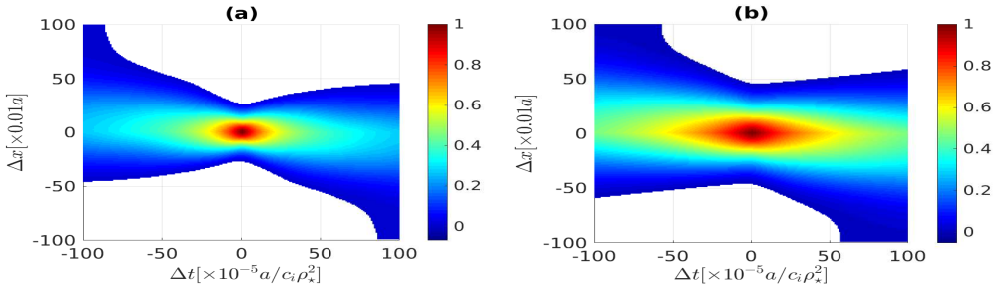

Figure 8. (a) 2d auto-correlation of intensity at $Pr = 1$. (b) 2d auto-correlation of intensity at $Pr = 6$. Plotted on log scale along z axis. Upper and lower boundaries are the locii of first zeroes of the correlation function. Slope of the boundary yields speed of the avalanches and sign of the slope indicates propagation direction. Different positive and negative slopes indicate asymmetry in speed of incoming and outgoing avalanches.

IV. SPREADING EFFECTS IN H MODE

A. Model for H mode studies

In H mode the $E \times B$ shearing is strong and transport bifurcation is important. So $E \times B$ shearing feedbacks are retained in the model equations(4)(5)and(6). We consider the unistable reaction term as $f = \chi \left[\left(\left|\frac{\partial P}{\partial x}\right| - \mu_c\right) \Theta \left(\left|\frac{\partial P}{\partial x}\right| - \mu_c\right) - \lambda V_E'^2\right] I - \beta I^2$ where the first term is critical pressure gradient driven linear growth rate reduced by $E \times B$ shear damping, μ_c is critical pressure gradient, Θ is Heaviside function. The second term is for nonlinear saturation of turbulence. The third term accounts for non-linear turbulence spreading. As explained in the previous section both second and third terms originate from $E \times B$ convective non-linearity upon applying a two scale closure. λ controls the strength of shear reduction, β controls the strength of non-linear saturation. With this the intensity evolution equation(4) reads

$$\frac{\partial I}{\partial t} = \chi \left[\left(\left|\frac{\partial P}{\partial x}\right| - \mu_c\right) \Theta \left(\left|\frac{\partial P}{\partial x}\right| - \mu_c\right) - \lambda V_E'^2\right] I - \beta I^2 + \sigma \frac{\partial}{\partial x} I \frac{\partial I}{\partial x} \tag{9}$$

where σ controls the strength of turbulence spreading. This is supplemented with pressure and density equations for completeness.

$$\frac{\partial P}{\partial t} = \frac{\partial}{\partial x}\left(\frac{\alpha_p I}{1+\epsilon V_E'^2} + D_{cp}\right)\frac{\partial P}{\partial x} + S_p \tag{10}$$

and

$$\frac{\partial n}{\partial t} = \frac{\partial}{\partial x}\left(\frac{\alpha_n I}{1+\epsilon V_E'^2} + D_{cn}\right)\frac{\partial n}{\partial x} + S_n \tag{11}$$

But one may ask why stick to such a primitive model when models such as those evolving 6 fields are already available[63]? *Note that our aim is not to rediscover the L-H mode transition but to understand and explore the effect of turbulence spreading on the pedestal in H mode.* 2-field models consisting of density and intensity or pressure and intensity fail to localize $E \times B$ shear towards the edge. Only a 3-field model (and beyond) self-consistently localizes the $E \times B$ shear towards the edge. This is because density remains flat at most of the locations except near edge. This model can be thought as an extension of that of Hinton-Staebler[35] here, with intensity as an additional field, or as a sub-set of a model due to Miki *et al*[64] without poloidal flow and zonal flow dynamics. The model equations(9),(10) and (11) are solved numerically using finite volume scheme for the boundary conditions $\frac{\partial I}{\partial x}(x = 0) = \frac{\partial I}{\partial x}(x = a) = 0$, $\frac{\partial n}{\partial x}(x = 0) = \frac{\partial P}{\partial x}(x = 0) = 0$, $n(x = a) = 0.01$ and $P(x = a) = 0$. We introduce normalizations similar to that used in Section(III) for the numerical simulations. Space and time is normalized as $x \to \hat{x} = x/a$, $t \to \hat{t} = tc_i\rho_\star^2/a$. P and n are normalized by reference values $P_0 = 1 \times 10^{19} KeVm^{-3}$ and $n_0[= 1 \times 10^{19} m^{-3}]$: $P \to \hat{P} = P/P_0$ and $n \to \hat{n} = n/n_0$. Further $V_E' \to \hat{V}_E' = V_E' a/c_i\rho_\star = -\frac{1}{\hat{n}^2}\frac{d\hat{P}}{d\hat{x}}\frac{d\hat{n}}{d\hat{x}}$. Turbulent diffusivities generally $\propto \chi_{GB}\frac{I}{\rho^{\star 2}}$. Hence this normalization leads to $\sigma \to \hat{\sigma} = \sigma/\chi_{GB}$, $\alpha_n \to \hat{\alpha}_n = \alpha/\chi_{GB}$, $\alpha_P \to \hat{\alpha}_P = \alpha_P/\chi_{GB}$, $D_{cP,cn} \to \hat{D}_{cP,cn} = D_{cP,cn}/\chi_{GB}$. The intensity is normalized as $I \to \hat{I} = I/\rho^{\star 2}$. Also $\chi \to \hat{\chi} = \chi a/c_i\rho_\star^2$, $(\lambda, \epsilon) \to (\hat{\lambda}, \hat{\epsilon}) = (\lambda, \epsilon)\rho_\star c_i^2/a^2$ and $\beta \to \hat{\beta} = \beta a/c_i$. Finally the sources are normalized as $S_n \to \hat{S}_n = aS_n/n_0 c_i \rho^{\star 2}$ and $S_P \to \hat{S}_P = aS_p/P_0 c_i \rho^{\star 2}$. The normalized equations look same as the original equations with "hatted" variables.

B. Pedestal/ H mode results

Figure(9) shows the variation of turbulence intensity, pressure and density profile with variation of the spreading strength $\hat{\sigma}$. It can be seen that width and height of both density

and pressure pedestals increase with $\hat{\sigma}$ at fixed pressure gradient. At the same time turbulence intensity in No Man's Land (NML) decreases. The reduction of intensity at NML is consistent with the finding of Hahm *et al*[10] that turbulence spreading into a linearly stable zone reduces the turbulence intensity in the unstable zone. Global confinement improves with $\hat{\sigma}$. Turbulence intensity is strongest in the NML, when spreading is weakest. Turbulence intensity decreases with $\hat{\sigma}$ leading to global confinement improvement. The intensity gradient is negative in NML and positive in the core. As a result turbulence spreading is radially outward in NML, and inward in the core region. The intensity gradient is stronger in NML than in the core. Consequently, outward spreading is stronger than inward spreading, which makes the intensity flux profile asymmetric. The outward spreading at NML increases, and inward spreading in core decreases with increasing $\hat{\sigma}$. This is shown in figure(10) where it can be observed that the in-out asymmetry in turbulence spreading increases with $\hat{\sigma}$. This explains why the turbulence in the NML is depleted faster than that in the core. Turbulence spreads from NML in to the pedestal, where it is dissipated by strong $E \times B$ shear. Thus the pedestal acts a sink of turbulence coming from NML, resulting in a reduction of total turbulence energy. *The pedestal expands in reaction to turbulence reduction in NML due to spreading. This leads to global confinement improvement.* However the pedestal is not completely free of turbulence - some turbulence survives in the vicinity of the pedestal top. The depth of penetration of turbulence increases with $\hat{\sigma}$. This means that the turbulence front propagating faster in NML ends up deeper in the pedestal.

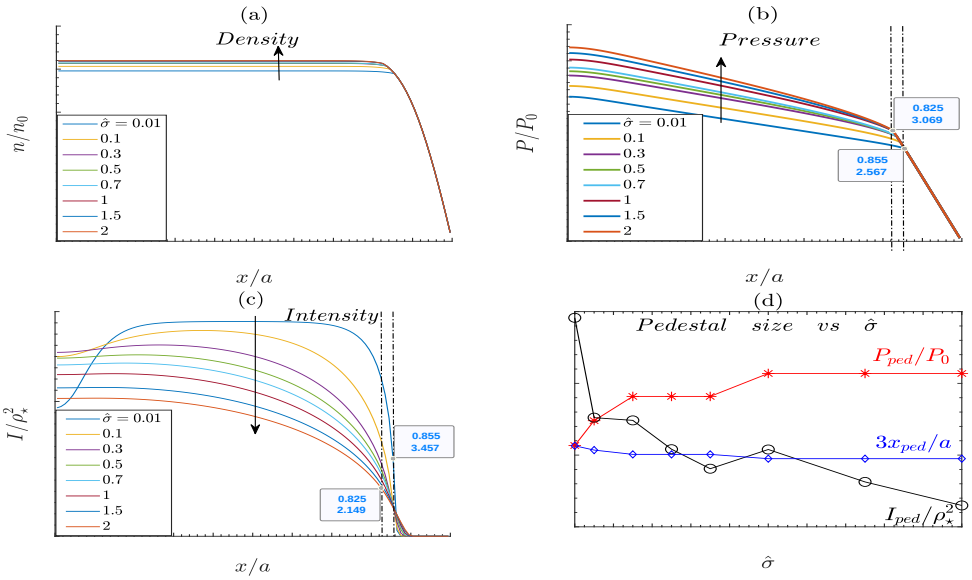

Figure 9. Results of model calculations with parameters $\hat{\chi} = 20$, $\mu_c = 1.2$, $\hat{\lambda} = 0.5$, $\hat{\beta} = 1$,$\hat{\alpha}_p = \hat{\alpha}_n = 0.5$, $\hat{D}_{cp} = \hat{D}_{cn} = 0.5$, $\hat{S}_p = 60e^{-100\hat{x}^2}$, $\hat{S}_n = 120e^{-100(\hat{x}-0.9)^2}$. Radial profiles of density(a), pressure(b), intensity(c). Variation of pedestal top pressure $\hat{P}_{ped}$, pedestal top intensity $\hat{I}_{ped}$ and pedestal top radial position $\hat{x}_{ped}$ is shown in (d). Arrows indicate trend of profiles with $\hat{\sigma}$.

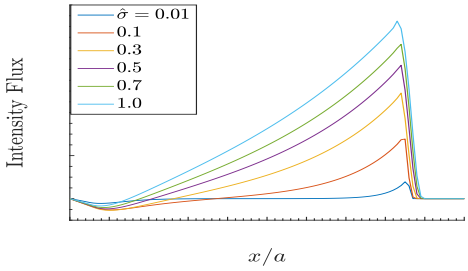

Figure 10. Normalized turbulence intensity flux with $\hat{\sigma}$.

Effect of additional non-diamagnetic shear- To test further the conclusion that the pedestal grows in reaction to turbulence reduction at NML, additional non-diamagnetic

shear V'_ϕ is added to the self-consistent diamagnetic shear V'_E localized within NML. We find that additional non-diamagnetic shear that adds to the diamagnetic $E \times B$ shear in NML elevates the pedestal by lowering the turbulence there. This is shown in figure(11). This means that controlling turbulence in the NML is the key to a wider pedestal, and hence confinement improvement.

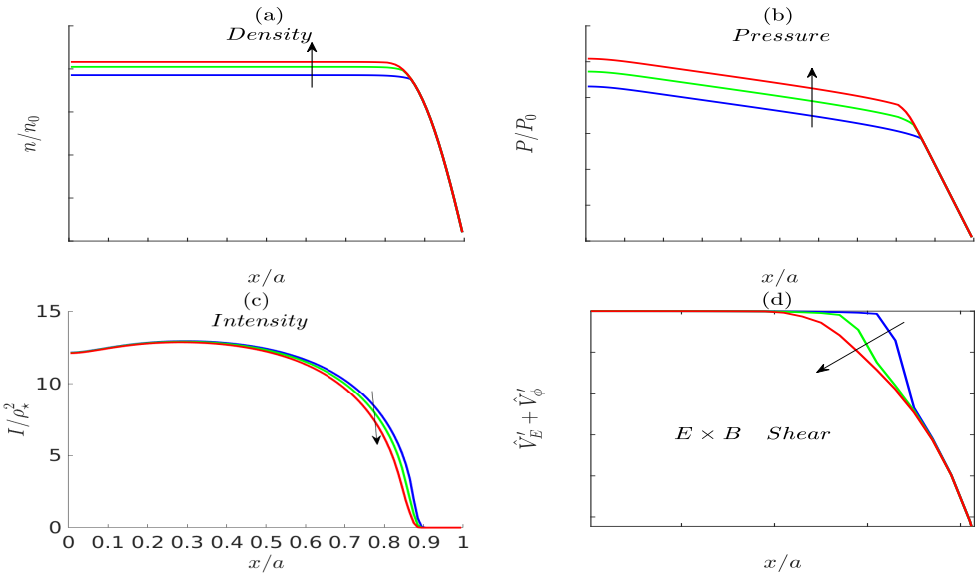

Figure 11. Results of model calculations with additional non-diamagnetic shear $\hat{V}'_\phi$ with parameters $\hat{\chi} = 20$, $\mu_c = 0$, $\hat{\lambda} = 0.5$, $\hat{\beta} = 1$, $\hat{\sigma} = 0.1$, $\hat{\alpha}_p = \hat{\alpha}_n = 0.5$, $\hat{D}_{cp} = \hat{D}_{cn} = 0.5$, $\hat{S}_p = 60e^{-100\hat{x}^2}$, $\hat{S}_n = 120e^{-100(\hat{x}-0.9)^2}$. Radial profiles of density(a), pressure(b), intensity(c) and $E \times B$ shear (d) are shown. Blue, green and red curves correspond to $\hat{V}'_\phi = 0$, $\hat{V}'_\phi = -1\,(\Theta(x-0.8) - \Theta(x-0.86))$ and $\hat{V}'_\phi = -2\,(\Theta(x-0.8) - \Theta(x-0.86))$ respectively. Arrows indicate trend of profiles with $\hat{V}'_\phi$. These plots clearly show that additional non-diamagnetic shear in NML reduces turbulence intensity and and elevates pedestal.

V. CONCLUSIONS AND DISCUSSIONS

We studied the effect of turbulence spreading on profile formation, with a special focus on steady state structure of profiles in L and H mode discharges. Minimal models are set up for numerical studies so as to isolate the effect of spreading. A 2-field model evolving turbulence intensity and pressure is employed to understand spreading effects on L mode profiles and avalanches. For H mode studies, a 3-field model self-consistently evolving intensity, pressure and density is used. Such a three field model is a bare minimum to study pedestal formation. Note that the density profile is mostly flat except near the edge. This helps in localizing the diamagnetic electric field shear near the edge - a necessary requirement for pedestal formation. The principal results of this paper are as follows:

- Turbulence spreading has an impact on profiles structure whenever there is a turbulence intensity gradient produced self-consistently with profiles or due to influx boundary condition.
- An intensity gradient induces a flux of intensity which leads to local reduction in fluctuation intensity and thus a steepening of the pressure profile.
- Spreading effect on profiles in L mode is *weak,* due to weak intensity gradient. Spreading effects become more visible with enhanced edge intensity, be it either due to an edge-localized source or due to turbulence invasion from the SOL. Edge pressure gradient and intensity exhibit a linear relation on a log-log scale(see figures(4) and(5)).
- The avalanche distribution is *weakly* affected by turbulence spreading as seen from frequency spectra of intensity fluctuations and fluxes. The sub-criticality parameter β *weakly* affects avalanche distribution(see figures(6),(7) and(8)).
- H mode profiles are *strongly* affected by turbulence spreading due to the strong intensity gradient at interface connecting barrier and core - i.e. No Man's Land. Turbulence spreads from the core (unstable zone) to the pedestal (stable zone) where it is suppressed by strong $E \times B$ shear. *Turbulence in NML is reduced, and pedestal height and the width increases in response to spreading.* Thus we see that turbulence spreading is *good* for H mode confinement(see figures(9) and (10)).

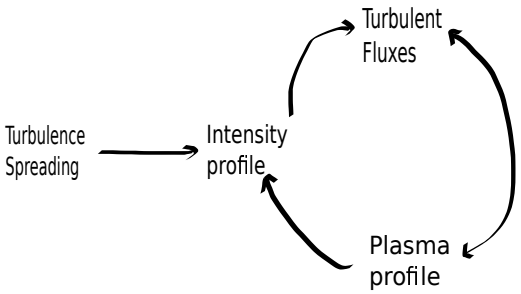

Figure 12. Schematic of spreading effect on profiles

- Additional non-diamagnetic $E \times B$ shear (such as that due toroidal rotation) added to diamagnetic $E \times B$ shear at NML elevates the pedestal by lowering the turbulence there. This means that controlling turbulence in the NML is *another way* to achieve a wider pedestal and hence confinement improvement(see figure(11)).

The turbulence spreading effects on profile discovered here with reduced models are also expected to apply to more comprehensive transport models, which include separate equations for ion and electron pressure, poloidal and toroidal momentum equations etc. Spreading changes the local intensity profile which affects turbulent fluxes. Plasma profiles are affected by turbulent fluxes and plasma profiles affect turbulent fluxes and local intensity. This is schematized in figure(12).

The most important finding of this paper is that the turbulence spreading enhances pedestal height and width. Thus spreading can have a positive impact on confinement in H mode. While this adds another dimension to the physics of pedestal size, it is extremely difficult to test in experiments because there is no unique control knob to turn spreading on/off. Even in simulations, it is still unclear as to how to separate spreading from spatially local energy transfer(cascading). Experimental measurements already include the effect of spreading. One can not have discharges with and without spreading. Spreading and nonlinear saturation both result from the ExB convective non linearity, which combines scattering in k-space and x-space respectively. This follows straightforwardly from a two-scale DIA closure of the ExB nonlinearity as shown in equation(2). Controlled spreading studies in nonlinear global GK simulations have yet to be achieved. Hence the findings of our reduced model provide impetus for deeper research on the physics of pedestal size. The results of this paper suggest

that spreading should be included in pedestal models. Having realized that the scattering in k and x are coupled, the only way to study the effect of spreading in reduced models is to vary it's strength by diffusivity parameter scans. This freedom is simply not available in the real experiments and non-linear simulations. In simulations, one can vary the sources (in flux driven case) or gradients (for gradient driven case). Of course, there is much evidence of turbulence spreading in experiments and simulations, identified by transient turbulence pulses and observation of turbulent transport in linearly stable region (see the review article by Hahm and Diamond[11] and the references therein for a comprehansive list). But none has identified how spreading affect profiles, possibly due to the afore-mentioned reasons. *No simulations or experiments, with controlled variation of spreading strength, exist to compare directly with our results.*

Nevertheless, there are a few works related to turbulence spreading that make tangential contact with some of the results obtained in this paper. These are discussed next with a focus on qualitative comparisons.

A recent full-f gyrokinetic simulations with GYSELA[65, 66] suggest that SOL asymmetry induces SOL flows which are unstable to parallel shear flow instability (PSFI). Such shear-driven fluctuations in turn energize edge turbulence. The resulting inward flux of turbulence creates a turbulence intensity profile that is monotonically increasing in radius as seen in tokamak experiments. Thus SOL turbulence and inward spreading of SOL turbulence have been identified as the important effects (in Refs[65, 66]) to explain the radially increasing turbulence intensity profile in L mode. This result is qualitatively similar to our L mode results presented in figures (4) and (5) obtained by using an edge localized source of intensity and/or inward flux of turbulence intensity at the edge. However it must be mentioned that the simulations in Refs[65, 66] do not include kinetic electrons and hence do not include the possibility of resistive-drift modes in the L-mode edge. It may be possible that significant local drive by resistive-drift mode in the edge region alters the intensity profile such that spreading from the SOL is not important. This can happen when resistive-drift mode driven local intensity in the edge region becomes comparable to PSFI driven turbulence intensity in the SOL region. Recent linear and nonlinear gyrokinetic analysis on AUG and JET cases has shown that local models are able to adequately describe the experimental flux levels[67]. This indicates that SOL turbulence invasion could be insignificant when resistive-drift mode is strongly excited in the edge region.

Fluid simulations in Ref[68] studied the effect of turbulence spreading on the pedestal immersed in interchange turbulence in the SOL and arrived at the conclusion that spreading shrinks the barrier width. This result looks opposite to our result on H mode. However one must be cautioned that the barrier in this work[68] is a "model" barrier formed by manually setting the interchange drive to zero in a radial domain. In contrast, the barrier in our study is formed by a transport bifurcation induced by radial electric field shear in H mode. Also, SOL turbulence spreading effect is not considered in our H mode calculations and is left for futre studies. This is for reasons of simplicity.

Finally, the pedestal widening effect of additional non-diamangetic ExB shear in NML, presented in figures(11), is qualitatively consistent with wide pedestal transition on torque ramp down in Q-H mode in DIII-D tokamak[69–71]. The torque ramp down modifies the ExB shear profile such that the ExB shearing rate increases at the pedestal top and decreases in the pedestal center. This leads to enhancement of pedestal width and height. See figure(3) in Ref[69], figure(14) in Ref[70] and figure(9) in Ref[71]. Of course, our model does not evolve toroidal and poloidal flows. The non-diamagnetic shear at NML is added manually to see its effect on local turbulence and pedestal size. This was done to test that the pedestal widening is actually due to reduction of turbulence intensity in NML. Turbulence reduction in NML, either by enhanced ExB shear in NML or by enhanced turbulence spreading, leads to a wider pedestal.

Turbulence intensity fluctuations are often observed to be non-Gaussian in experiments. In this light, one could also construct a CTRW (continuous time random walk) model for turbulence spreading. In Fokker Planck approach the time step is fixed, acts like a clock. In CTRW time steps are no longer fixed and evolve dynamically as the walker position does. For separable joint probability distribution function (pdf)

$$\xi(x-x',x';t-t',t) = p(x-x',x';t)\psi(x';t-t')$$

, where p is for step size pdf and ψ is for waiting time pdf, one can expect to get an intensity evolution equation with the diffusion part replaced by

$$\int_0^t dt' \left[\int dx' \phi(x';t-t') p(x-x',x';t) I(x',t') - \phi(x;t-t') I(x,t') \right]$$

Here $\phi(x;t-t')$ is memory function and is related to the inhomogeneous waiting time pdf $\psi(x;t-t')$ through their Laplace transforms as $\phi(x;s) = s\psi(x,s)\left[1-\psi(x,s)\right]^{-1}$. This makes

the intensity evolution highly non-local in both space and time. Note that ϕ becomes a delta function only when the CTRW is Markovian. Further discussion on choice of step size and waiting time pdfs, and a formal derivation of a CTRW model for turbulence spreading will be presented elsewhere.

ACKNOWLEDGMENTS

The authors are grateful to Ö D Gürcan and G. Dif-Pradalier for useful discussions. We also acknowledge fruitful interactions with the participants in the Festival de Theorie 2019, Aix-en- Provence. This work was supported by US DOE under the award number $DE-FG02-04ER54738$.

Appendix A: Spreading term in the intensity equation

The second term on the r.h.s of equation(4) is negative of divergence of intensity flux $-\frac{\partial \Gamma_I}{\partial x}$, where the intensity flux is given by $\Gamma_I = -\sigma I \frac{\partial I}{\partial x}$. The diverence of flux can be expanded as follows

$$\frac{\partial}{\partial x}\sigma I \frac{\partial I}{\partial x} = \sigma I \frac{\partial^2 I}{\partial x^2} + \sigma \left(\frac{\partial I}{\partial x}\right)^2$$

. One might think that this produces a source term $\sigma \left(\frac{\partial I}{\partial x}\right)^2$ in the intensity equation. However, such can be re-absorbed again in the form of a divergence of a flux, as

$$\sigma I \frac{\partial^2 I}{\partial x^2} + \sigma \left(\frac{\partial I}{\partial x}\right)^2 = \frac{\partial}{\partial x}\sigma I \frac{\partial I}{\partial x}$$

. The term $\sigma \left(\frac{\partial I}{\partial x}\right)^2$ can be classified to an intensity gradient dependent reaction term or nonlinear advection term. It is only a part of the total contribution to the divergence of flux. There is no source term in the intensity equation(4). A true source term for I is one that does not depend on I or I' itself.

[1] D. Barkley, B. Song, V. Mukund, G. Lemoult, M. Avila, and B. Hof, Nature **526**, 550 (2015).

[2] M. Couliou and R. Monchaux, Phys. Rev. E **93**, 013108 (2016).

[3] X. Garbet, L. Laurent, A. Samain, and J. Chinardet, Nuclear Fusion **34**, 963 (1994).

[4] R. D. Sydora, V. K. Decyk, and J. M. Dawson, Plasma Physics and Controlled Fusion **38**, A281 (1996).

[5] S. E. Parker, H. E. Mynick, M. Artun, J. C. Cummings, V. Decyk, J. V. Kepner, W. W. Lee, and W. M. Tang, Physics of Plasmas **3**, 1959 (1996), https://doi.org/10.1063/1.871992.

[6] Y. Kishimoto, T. Tajima, W. Horton, M. J. LeBrun, and J. Y. Kim, Physics of Plasmas **3**, 1289 (1996), https://doi.org/10.1063/1.871754.

[7] W. W. Lee and R. A. Santoro, Physics of Plasmas **4**, 169 (1997), https://doi.org/10.1063/1.872128.

[8] Z. Lin and T. S. Hahm, Phys. Plasmas **11**, 1099 (2004).

[9] Z. Lin, S. Ethier, T. S. Hahm, and W. M. Tang, Phys. Rev. Lett. **88**, 195004 (2002).

[10] T. S. Hahm, P. H. Diamond, Z. Lin, K. Itoh, and S.-I. Itoh, Plasma Physics and Controlled Fusion **46**, A323 (2004).

[11] T. S. Hahm and P. H. Diamond, J. Kor. Phys. Soc. **73**, 747 (2018).

[12] M. Yagi, T. Ueda, S.-I. Itoh, M. Azumi, K. Itoh, P. H. Diamond, and T. S. Hahm, Plasma Physics and Controlled Fusion **48**, A409 (2006).

[13] E. Poli, A. Bottino, and A. Peeters, Nuclear Fusion **49**, 075010 (2009).

[14] E. Poli, A. Bottino, W. A. Hornsby, A. G. Peeters, T. Ribeiro, B. D. Scott, and M. Siccinio, Plasma Physics and Controlled Fusion **52**, 124021 (2010).

[15] M. Choi, J. Kim, J.-M. Kwon, H. Park, Y. In, W. Lee, K. Lee, G. Yun, J. Lee, M. Kim, W.-H. Ko, J. Lee, Y. Park, Y.-S. Na, N. Luhmann, and B. Park, Nuclear Fusion **57**, 126058 (2017).

[16] K. Ida, T. Kobayashi, M. Ono, T. E. Evans, G. R. McKee, and M. E. Austin, Phys. Rev. Lett. **120**, 245001 (2018).

[17] S. Kaye, F. Levinton, D. Stutman, K. Tritz, H. Yuh, M. Bell, R. Bell, C. Domier, D. Gates, W. Horton, J. Kim, B. LeBlanc, N. Luhmann, R. Maingi, E. Mazzucato, J. Menard, D. Mikkelsen, D. Mueller, H. Park, G. Rewoldt, S. Sabbagh, D. Smith, and W. Wang, Nuclear Fusion **47**, 499 (2007).

[18] R. Nazikian, K. Shinohara, G. J. Kramer, E. Valeo, K. Hill, T. S. Hahm, G. Rewoldt, S. Ide, Y. Koide, Y. Oyama, H. Shirai, and W. Tang, Phys. Rev. Lett. **94**, 135002 (2005).

[19] G. R. McKEE, R. J. FONCK, D. K. GUPTA, D. J. SCHLOSSBERG, M. W. SHAFER, R. L. BOIVIN, and W. SOLOMON, Plasma and Fusion Research **2**, S1025 (2007).

[20] T. Estrada, C. Hidalgo, and T. Happel, Nuclear Fusion **51**, 032001 (2011).

[21] C. Holland, A. E. White, G. R. McKee, M. W. Shafer, J. Candy, R. E. Waltz, L. Schmitz, and G. R. Tynan, Physics of Plasmas **16**, 052301 (2009), https://doi.org/10.1063/1.3085792.

[22] T. Rhodes, C. Holland, S. Smith, A. White, K. Burrell, J. Candy, J. DeBoo, E. Doyle, J. Hillesheim, J. Kinsey, G. McKee, D. Mikkelsen, W. Peebles, C. Petty, R. Prater, S. Parker, Y. Chen, L. Schmitz, G. Staebler, R. Waltz, G. Wang, Z. Yan, and L. Zeng, Nuclear Fusion **51**, 063022 (2011).

[23] N. T. Howard, A. E. White, M. Greenwald, M. L. Reinke, J. Walk, C. Holland, J. Candy, and T. Görler, Physics of Plasmas **20**, 032510 (2013), https://doi.org/10.1063/1.4795301.

[24] T. Görler, A. E. White, D. Told, F. Jenko, C. Holland, and T. L. Rhodes, Physics of Plasmas **21**, 122307 (2014), https://doi.org/10.1063/1.4904301.

[25] R. A. Fisher, Annals of Eugenics **7**, 355 (1937).

[26] A. Kolmogoroff, I. Petrovsky, and N. Piscounoff, Clin. Cancer Res. **1**, 1 (1937).

[27] X. Garbet, Y. Sarazin, F. Imbeaux, P. Ghendrih, C. Bourdelle, 3. D. Gürcan, and P. H. Diamond, Physics of Plasmas **14**, 122305 (2007), https://doi.org/10.1063/1.2824375.

[28] V. Naulin, A. H. Nielsen, and J. J. Rasmussen, Physics of Plasmas **12**, 122306 (2005), https://doi.org/10.1063/1.2141396.

[29] Z. Wang, P. Diamond, 3. Gürcan, X. Garbet, and X. Wang, Nuclear Fusion **51**, 073009 (2011).

[30] Ö. D. Gürcan, P. H. Diamond, T. S. Hahm, and Z. Lin, Phys. Plasmas **12**, 032303 (2005).

[31] S. Yi, J. M. Kwon, P. H. Diamond, and T. S. Hahm, Physics of Plasmas **21**, 092509 (2014), https://doi.org/10.1063/1.4896059.

[32] R. E. Waltz and J. Candy, Physics of Plasmas **12**, 072303 (2005), https://doi.org/10.1063/1.1947467.

[33] W. X. Wang, T. S. Hahm, W. W. Lee, G. Rewoldt, J. Manickam, and W. M. Tang, Physics of Plasmas **14**, 072306 (2007), https://doi.org/10.1063/1.2750647.

[34] W. Deng and Z. Lin, Physics of Plasmas **16**, 102503 (2009), https://doi.org/10.1063/1.3243918.

[35] F. L. Hinton and G. M. Staebler, Phys. Fluids B **5**, 1281 (1993).

[36] T. Kobayashi, K. Itoh, T. Ido, K. Kamiya, S.-I. Itoh, Y. Miura, Y. Nagashima, A. Fujisawa, S. Inagaki, K. Ida, and K. Hoshino, Sci. Rep. **6**, 30720 (2016).

[37] T. Kobayashi, K. Itoh, T. Ido, K. Kamiya, S.-I. Itoh, Y. Miura, Y. Nagashima, A. Fujisawa, S. Inagaki, and K. Ida, Scientific Reports **7**, 14971 (2017).

[38] P. Snyder, R. Groebner, J. Hughes, T. Osborne, M. Beurskens, A. Leonard, H. Wilson, and X. Xu, Nuclear Fusion **51**, 103016 (2011).

[39] H. Sugama and M. Wakatani, Journal of the Physical Society of Japan **61**, 3166 (1992), https://doi.org/10.1143/JPSJ.61.3166.

[40] E. jin Kim, P. Diamond, M. Malkov, T. Hahm, K. Itoh, S.-I. Itoh, S. Champeaux, I. Gruzinov, O. Gurcan, C. Holland, M. Rosenbluth, and A. Smolyakov, Nuclear Fusion **43**, 961 (2003).

[41] W. Horton, Rev. Mod. Phys. **71**, 735 (1999).

[42] R. Nazikian, K. Shinohara, G. J. Kramer, E. Valeo, K. Hill, T. S. Hahm, G. Rewoldt, S. Ide, Y. Koide, Y. Oyama, H. Shirai, and W. Tang, Phys. Rev. Lett. **94**, 135002 (2005).

[43] R. A. Heinonen and P. H. Diamond, Physics of Plasmas **26**, 030701 (2019), https://doi.org/10.1063/1.5083176.

[44] S. A. Orszag and A. T. Patera, Journal of Fluid Mechanics **128**, 347?385 (1983).

[45] Y. Pomeau, Comptes Rendus Mécanique **343**, 210 (2015).

[46] S. Inagaki, T. Tokuzawa, N. Tamura, S.-I. Itoh, T. Kobayashi, K. Ida, T. Shimozuma, S. Kubo, K. Tanaka, T. Ido, A. Shimizu, H. Tsuchiya, N. Kasuya, Y. Nagayama, K. Kawahata, S. Sudo, H. Yamada, A. Fujisawa, and K. I. and, Nuclear Fusion **53**, 113006 (2013).

[47] M. van Berkel, G. Vandersteen, H. Zwart, G. Hogeweij, J. Citrin, E. Westerhof, D. Peumans, and M. de Baar, Nuclear Fusion **58**, 106042 (2018).

[48] D. Biskamp and M. Walter, Physics Letters A **109**, 34 (1985).

[49] J. F. Drake, A. Zeiler, and D. Biskamp, Phys. Rev. Lett. **75**, 4222 (1995).

[50] B. Friedman and T. A. Carter, Physics of Plasmas **22**, 012307 (2015), https://doi.org/10.1063/1.4905863.

[51] B. D. Scott, Phys. Rev. Lett. **65**, 3289 (1990).

[52] B. D. Scott, Physics of Fluids B: Plasma Physics **4**, 2468 (1992), https://doi.org/10.1063/1.860215.

[53] Z. B. Guo and P. H. Diamond, Physics of Plasmas **24**, 100705 (2017), https://doi.org/10.1063/1.5000850.

[54] M. Barnes, F. I. Parra, E. G. Highcock, A. A. Schekochihin, S. C. Cowley, and C. M. Roach, Phys. Rev. Lett. **106**, 175004 (2011).

[55] F. van Wyk, E. G. Highcock, A. A. Schekochihin, C. M. Roach, A. R. Field, and W. Dorland, Journal of Plasma Physics **82**, 905820609 (2016).

[56] P. W. Terry, P. H. Diamond, and T. S. Hahm, Physics of Fluids B: Plasma Physics **2**, 2048 (1990), https://doi.org/10.1063/1.859426.

[57] M. Lesur and P. H. Diamond, Phys. Rev. E **87**, 031101 (2013).

[58] T. Hwa and M. Kardar, Phys. Rev. A **45**, 7002 (1992).

[59] D. E. Newman, B. A. Carreras, P. H. Diamond, and T. S. Hahm, Physics of Plasmas **3**, 1858 (1996), https://doi.org/10.1063/1.871681.

[60] B. A. Carreras, D. Newman, V. E. Lynch, and P. H. Diamond, Physics of Plasmas **3**, 2903 (1996), https://doi.org/10.1063/1.871650.

[61] J. A. Mier, L. García, and R. Sánchez, Physics of Plasmas **13**, 102308 (2006), https://doi.org/10.1063/1.2359285.

[62] Y. Sarazin, V. Grandgirard, J. Abiteboul, S. Allfrey, X. Garbet, P. Ghendrih, G. Latu, A. Strugarek, and G. Dif-Pradalier, Nuclear Fusion **50**, 054004 (2010).

[63] M. A. Malkov, P. H. Diamond, K. Miki, J. E. Rice, and G. R. Tynan, Physics of Plasmas **22**, 032506 (2015), https://doi.org/10.1063/1.4914934.

[64] K. Miki, P. H. Diamond, 3. D. Gürcan, G. R. Tynan, T. Estrada, L. Schmitz, and G. S. Xu, Physics of Plasmas **19**, 092306 (2012), https://doi.org/10.1063/1.4753931.

[65] G. Dif-Pradalier, E. Caschera, P. Ghendrih, Y. Asahi, P. Donnel, X. Garbet, C. Gillot, V. Grandgirard, G. Latu, C. Passeron, Y. Sarazin, and D. Zarzoso, ITPA (2019).

[66] Y. Sarazin, Festival de Theorie (2019), http://festival-theorie.org/y-sarazin-impact-of-asymmetries-on-transport-in-tokamak-plasmas/.

[67] N. Bonanomi, C. Angioni, P. Crandall, A. D. Siena, C. Maggi, P. Schneider, , and and, Nuclear Fusion **59**, 126025 (2019).

[68] P. Ghendrih, Y. Sarazin, G. Ciraolo, G. Darmet, X. Garbet, V. Grangirard, P. Tamain, S. Benkadda, and P. Beyer, Journal of Nuclear Materials **363-365**, 581 (2007), plasma-Surface Interactions-17.

[69] K. H. Burrell, K. Barada, X. Chen, A. M. Garofalo, R. J. Groebner, C. M. Muscatello, T. H. Osborne, C. C. Petty, T. L. Rhodes, P. B. Snyder, W. M. Solomon, Z. Yan, and L. Zeng, Physics of Plasmas **23**, 056103 (2016), https://doi.org/10.1063/1.4943521.

[70] X. Chen, K. Burrell, T. Osborne, W. Solomon, K. Barada, A. Garofalo, R. Groebner, N. Luhmann, G. McKee, C. Muscatello, M. Ono, C. Petty, M. Porkolab, T. Rhodes, J. Rost, P. Snyder, G. Staebler, B. Tobias, and Z. Y. and, Nuclear Fusion **57**, 022007 (2016).

[71] X. Chen, K. Burrell, T. Osborne, K. Barada, N. Ferraro, A. Garofalo, R. Groebner, G. McKee, C. Petty, M. Porkolab, T. Rhodes, J. Rost, P. Snyder, W. Solomon, and Z. Y. and, Nuclear Fusion **57**, 086008 (2017).

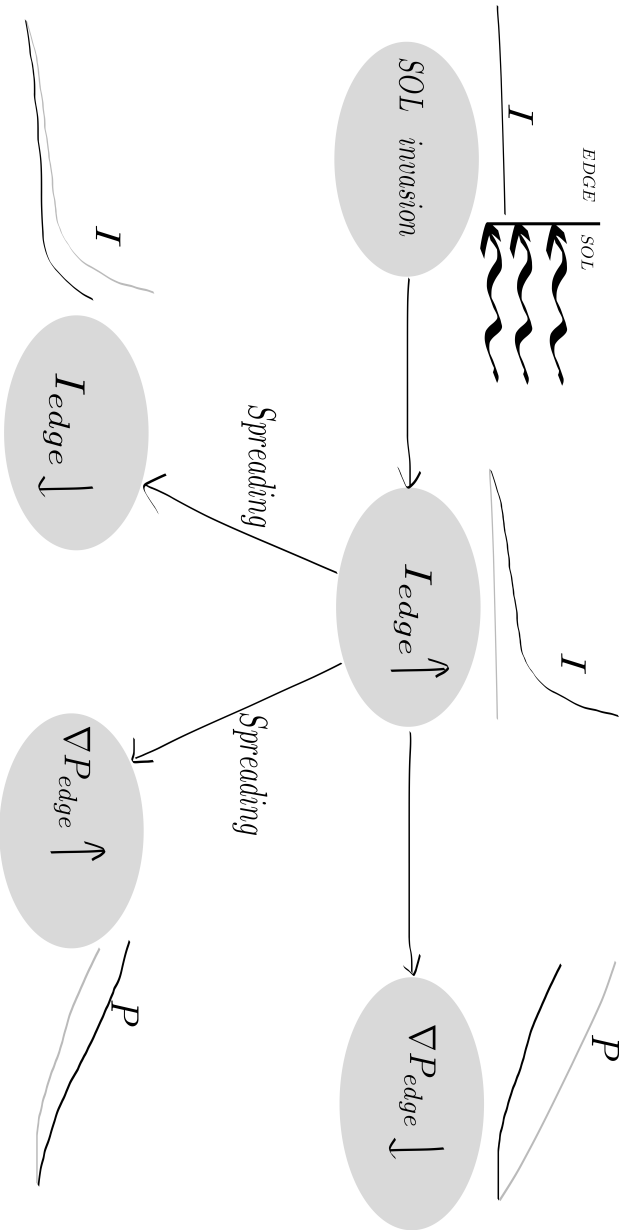

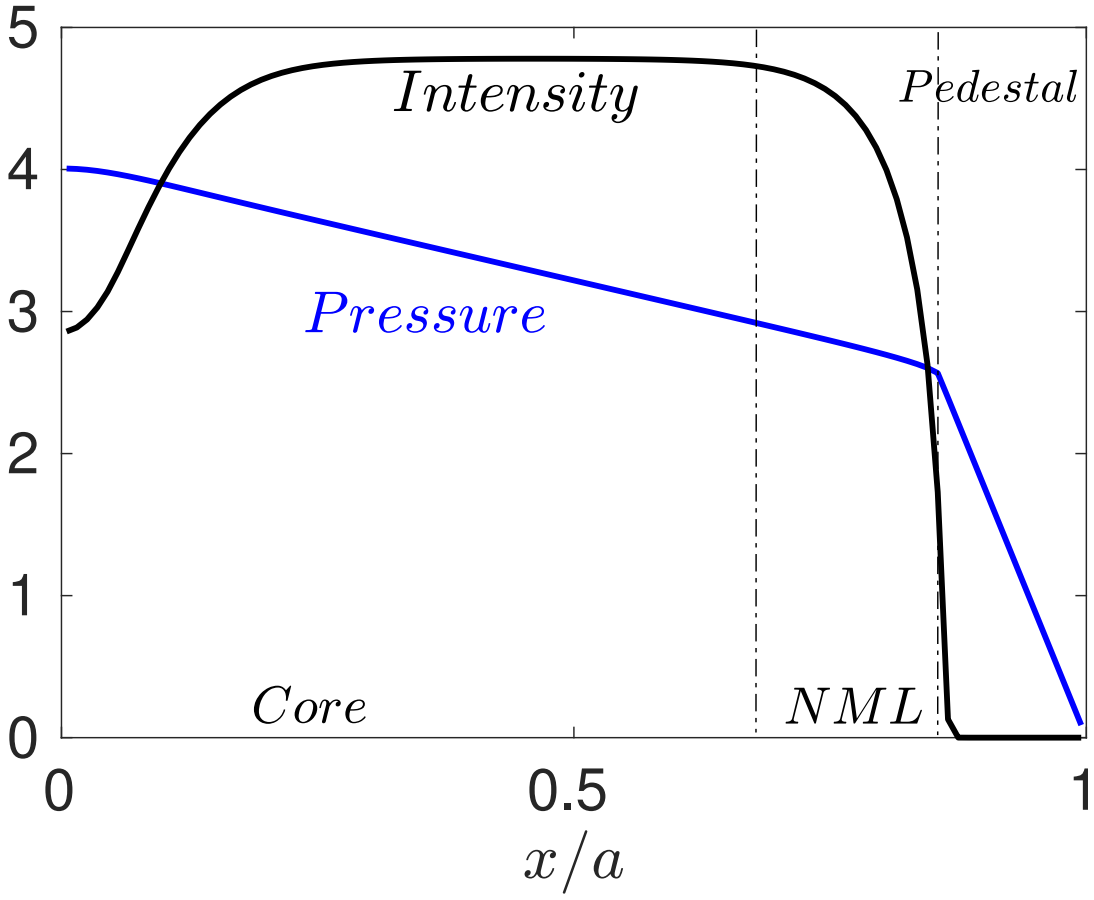

PLEASE CITE THIS ARTICLE AS DOI: 10.1063/1.5117835

PLEASE CITE THIS ARTICLE AS DOI: 10.1063/1.5117835

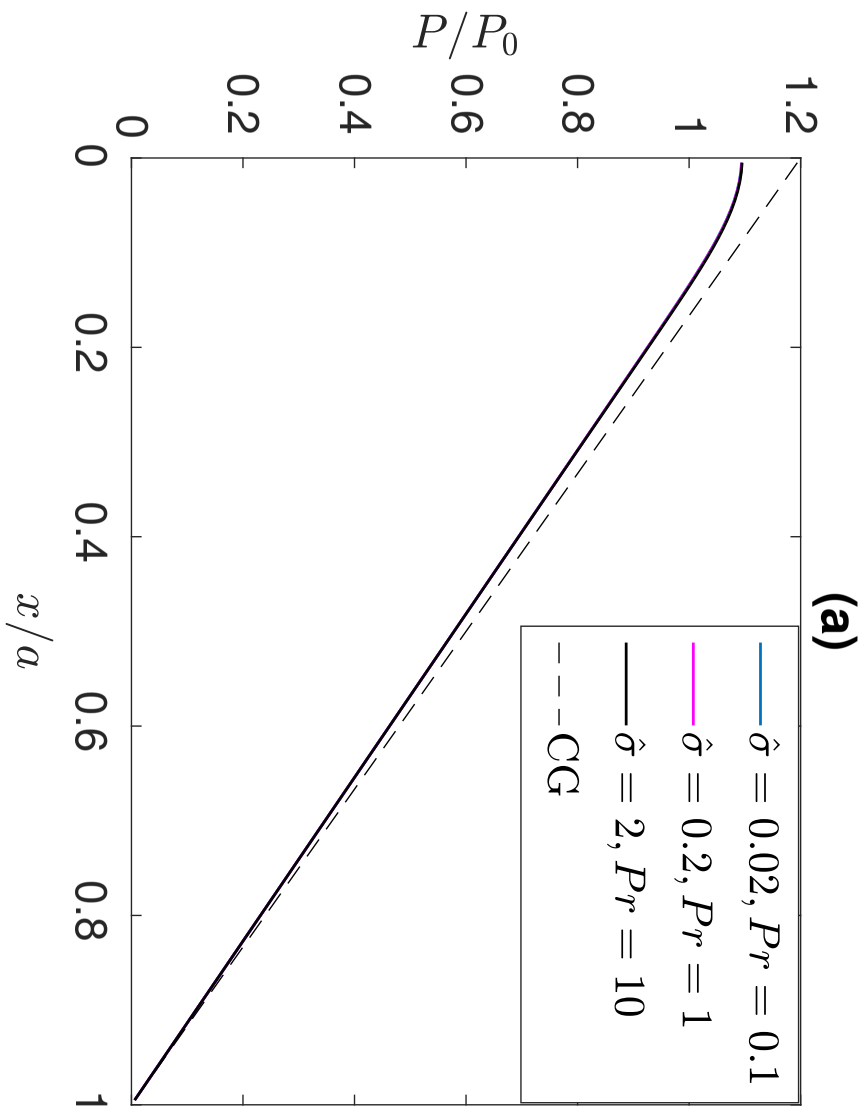

PLEASE CITE THIS ARTICLE AS DOI: 10.1063/1.5117835

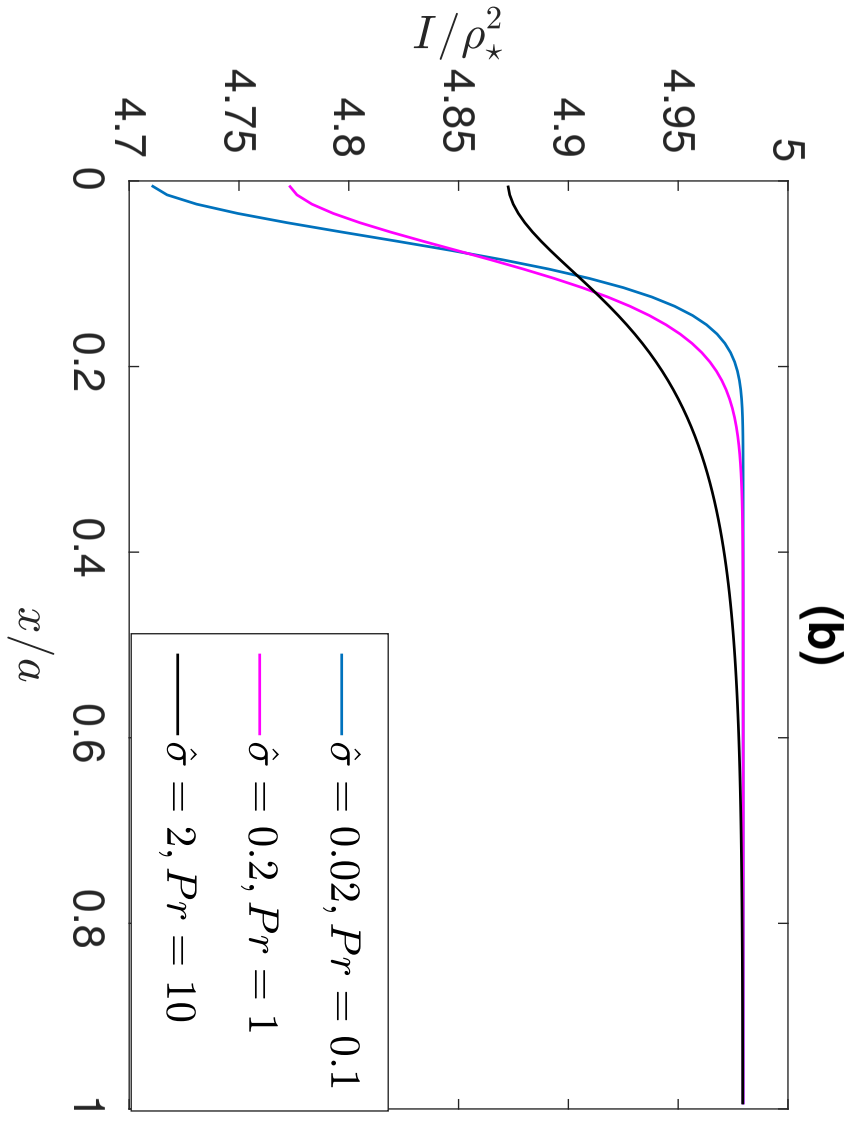

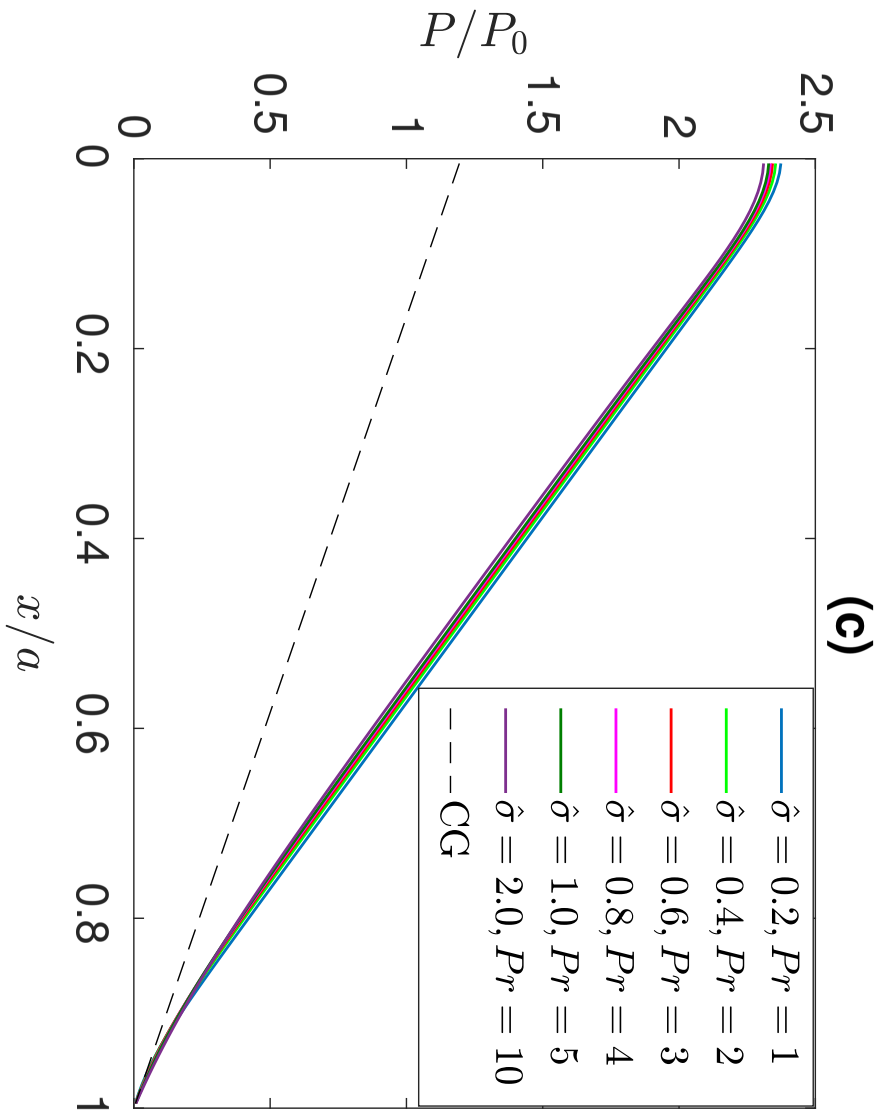

PLEASE CITE THIS ARTICLE AS DOI: 10.1063/1.5117835

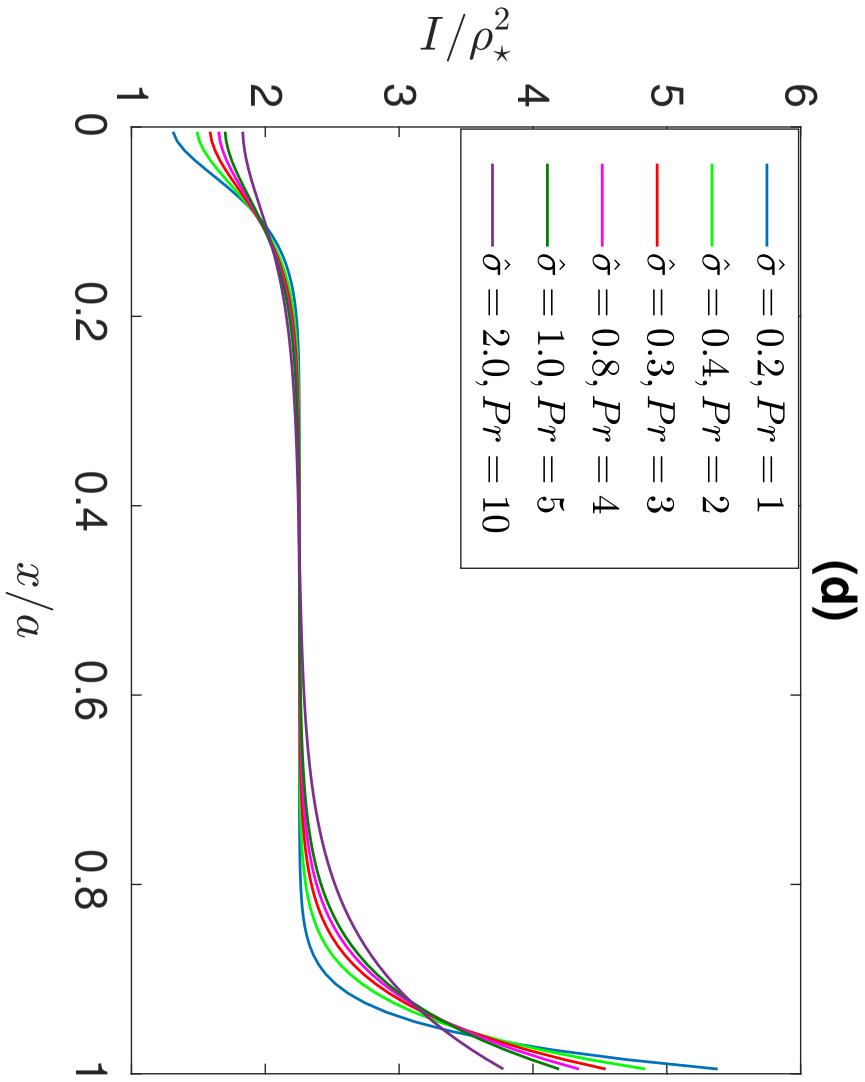

PLEASE CITE THIS ARTICLE AS DOI: 10.1063/1.5117835

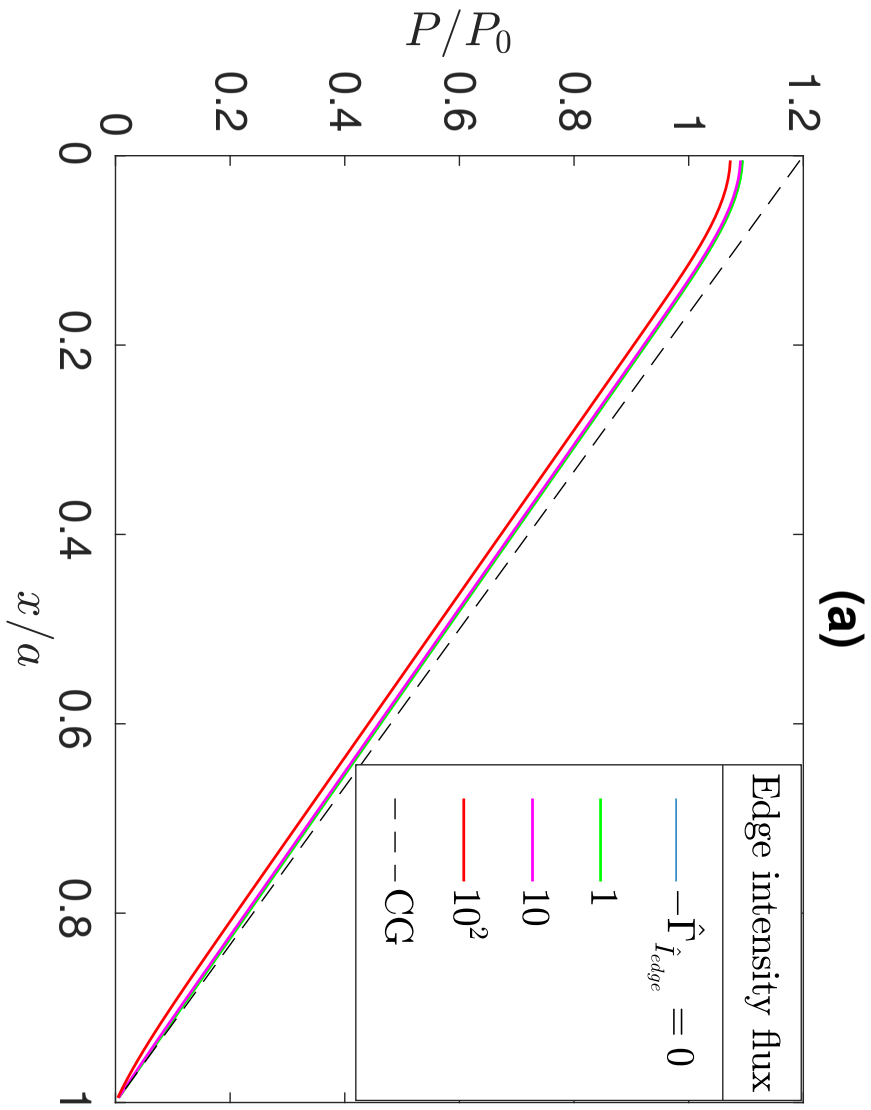

PLEASE CITE THIS ARTICLE AS DOI: 10.1063/1.5117835

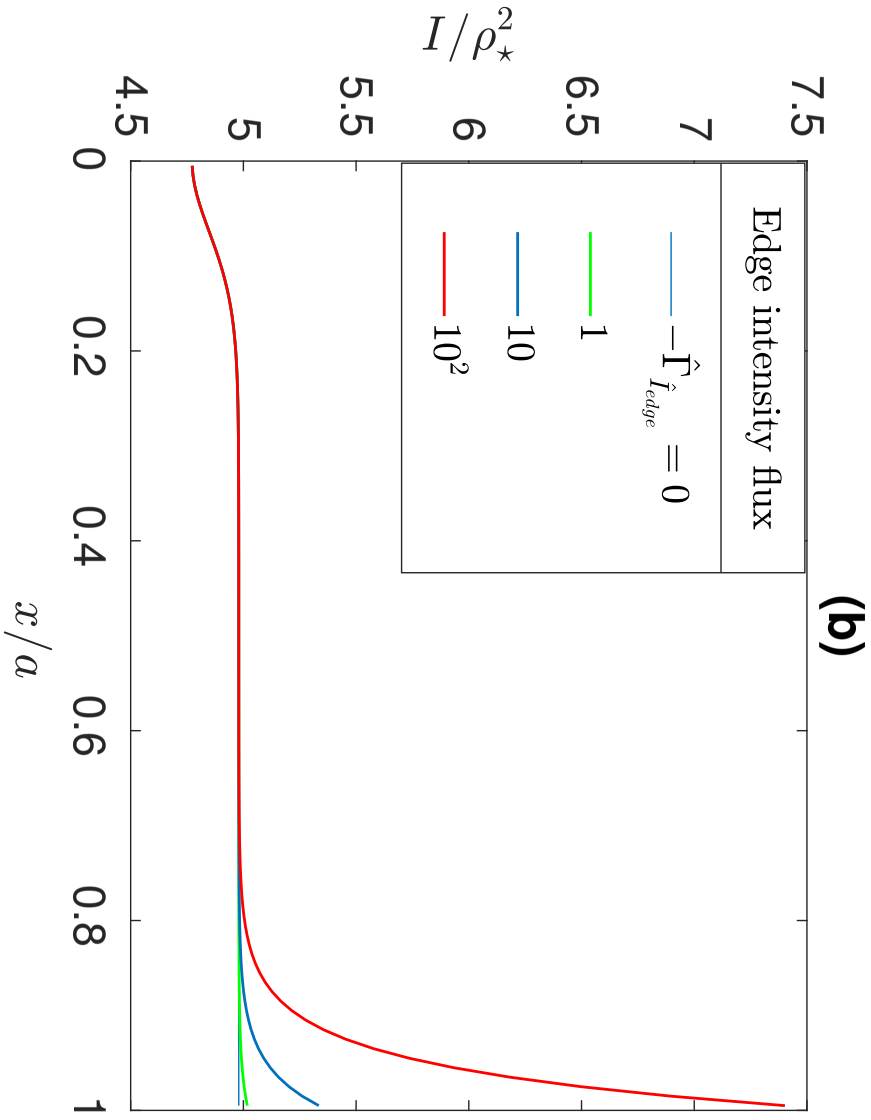

PLEASE CITE THIS ARTICLE AS DOI: 10.1063/1.5117835

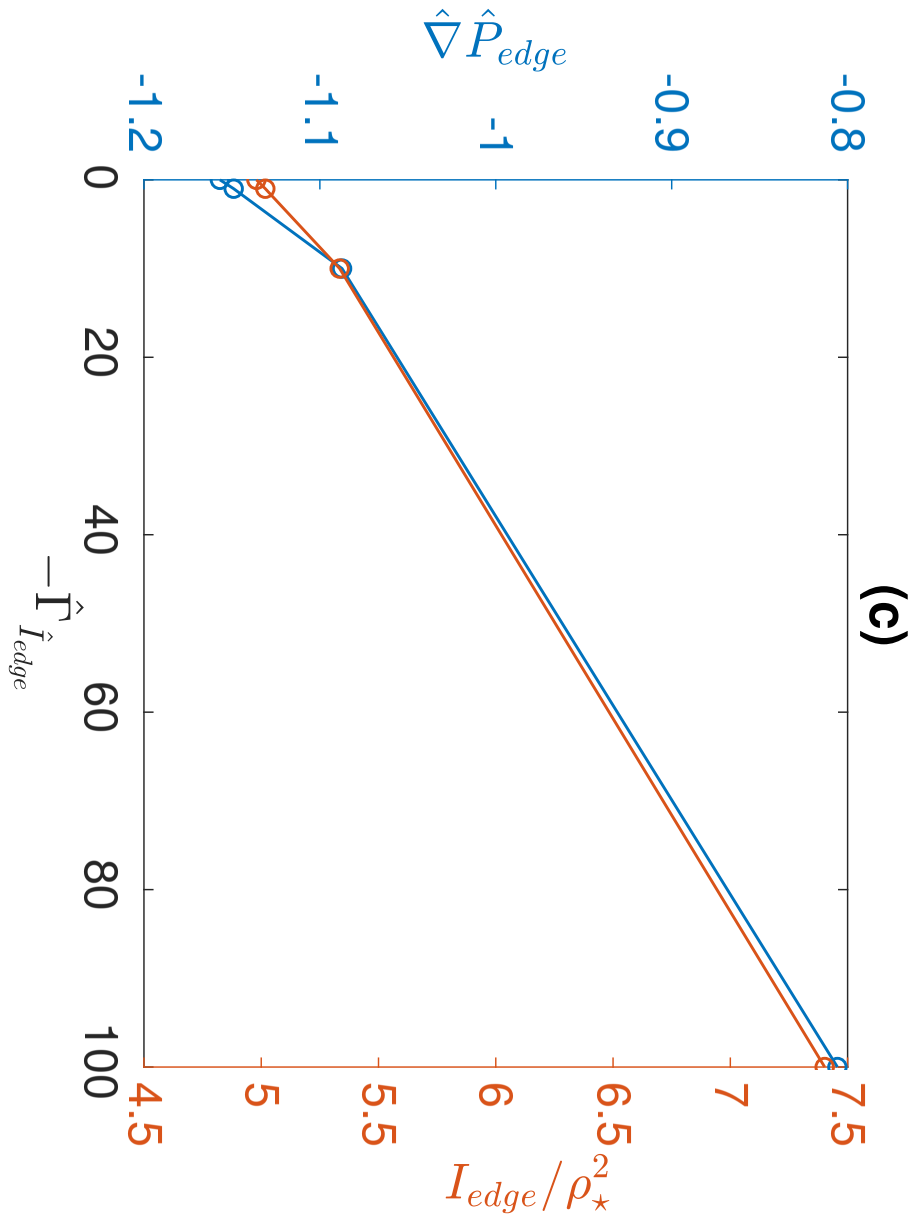

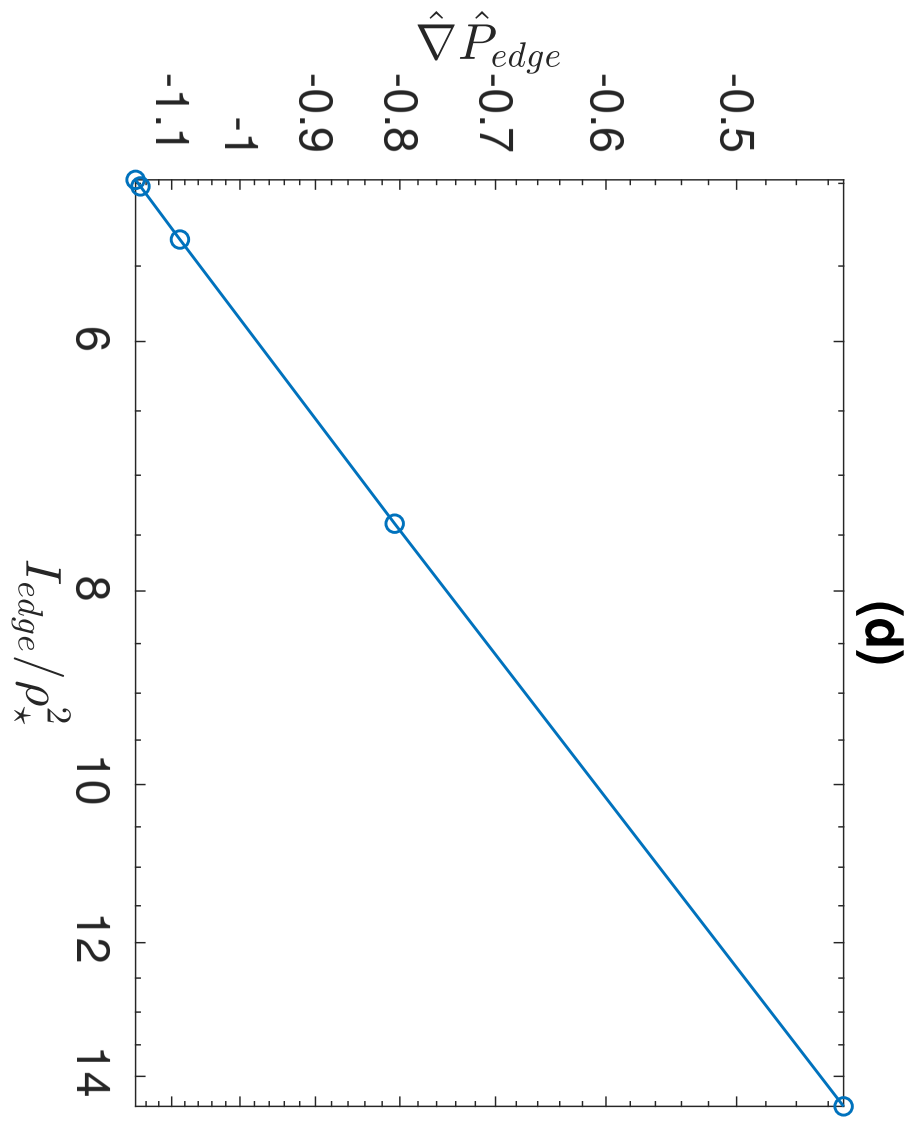

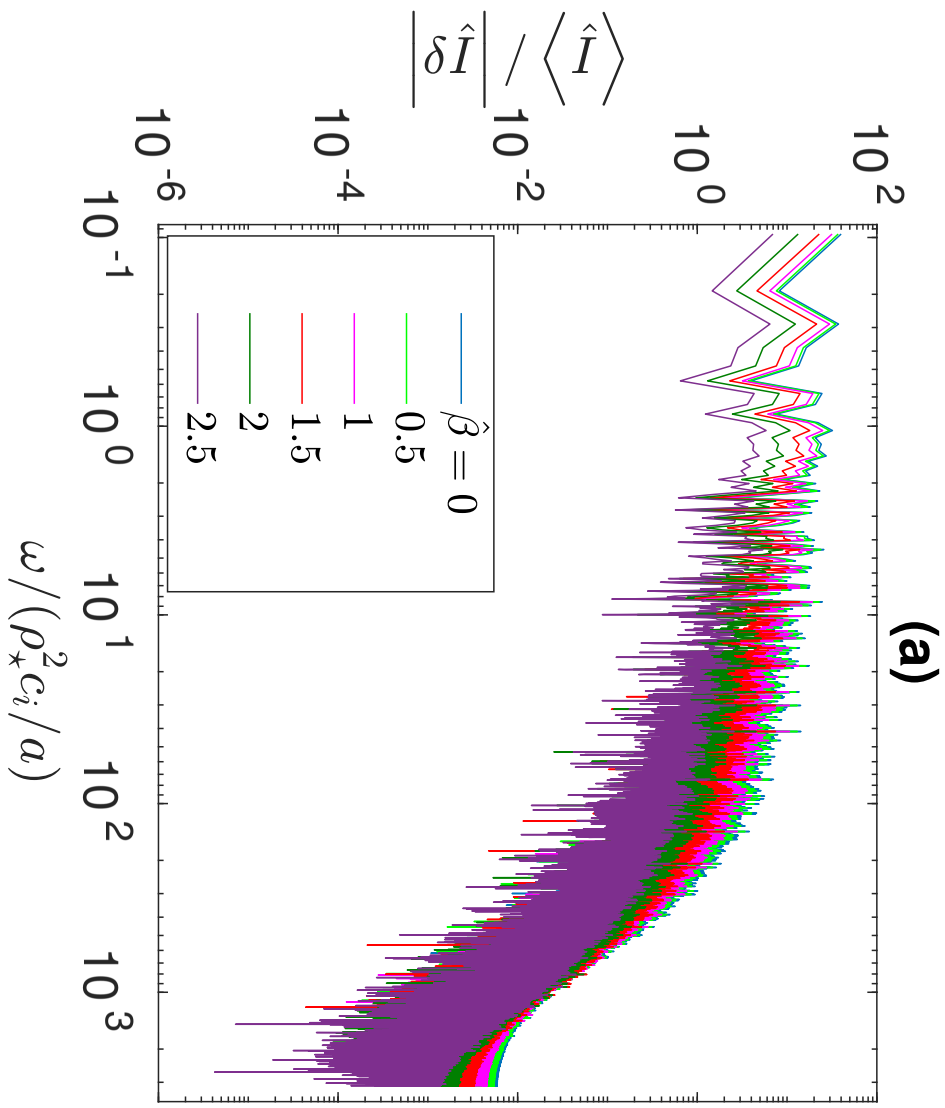

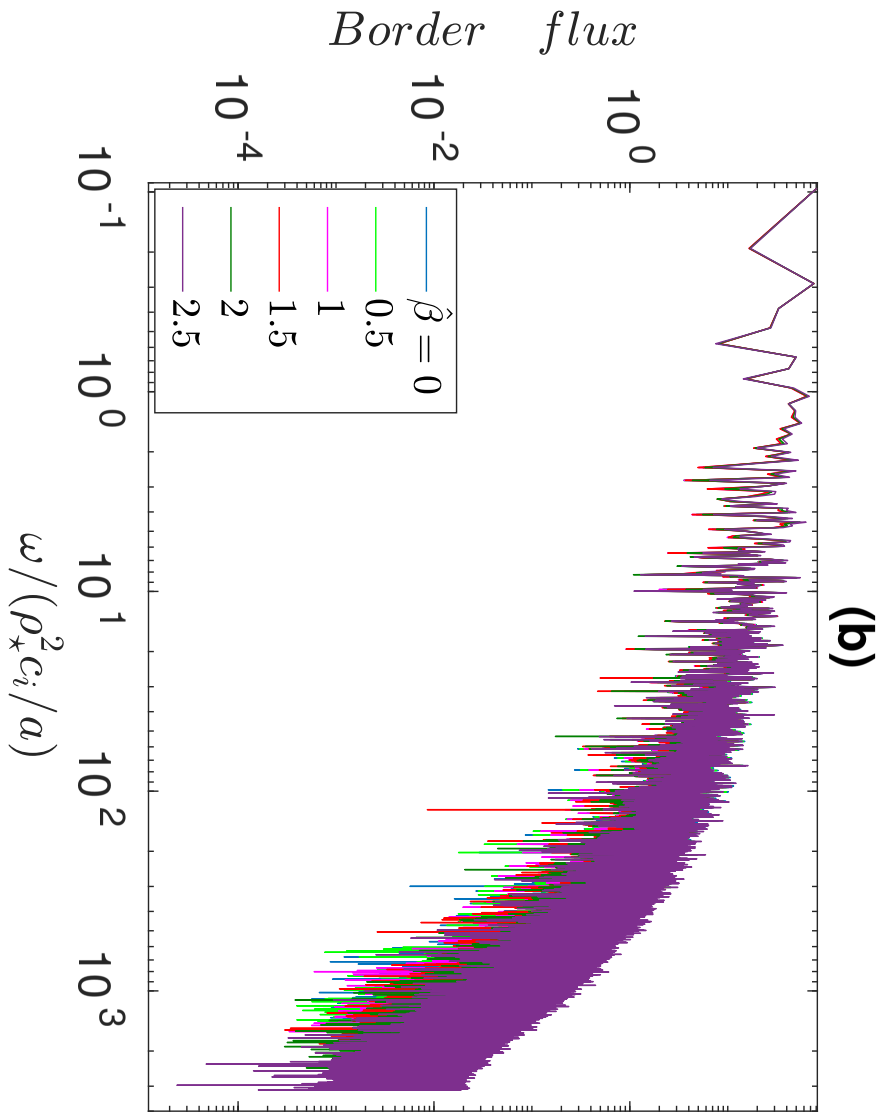

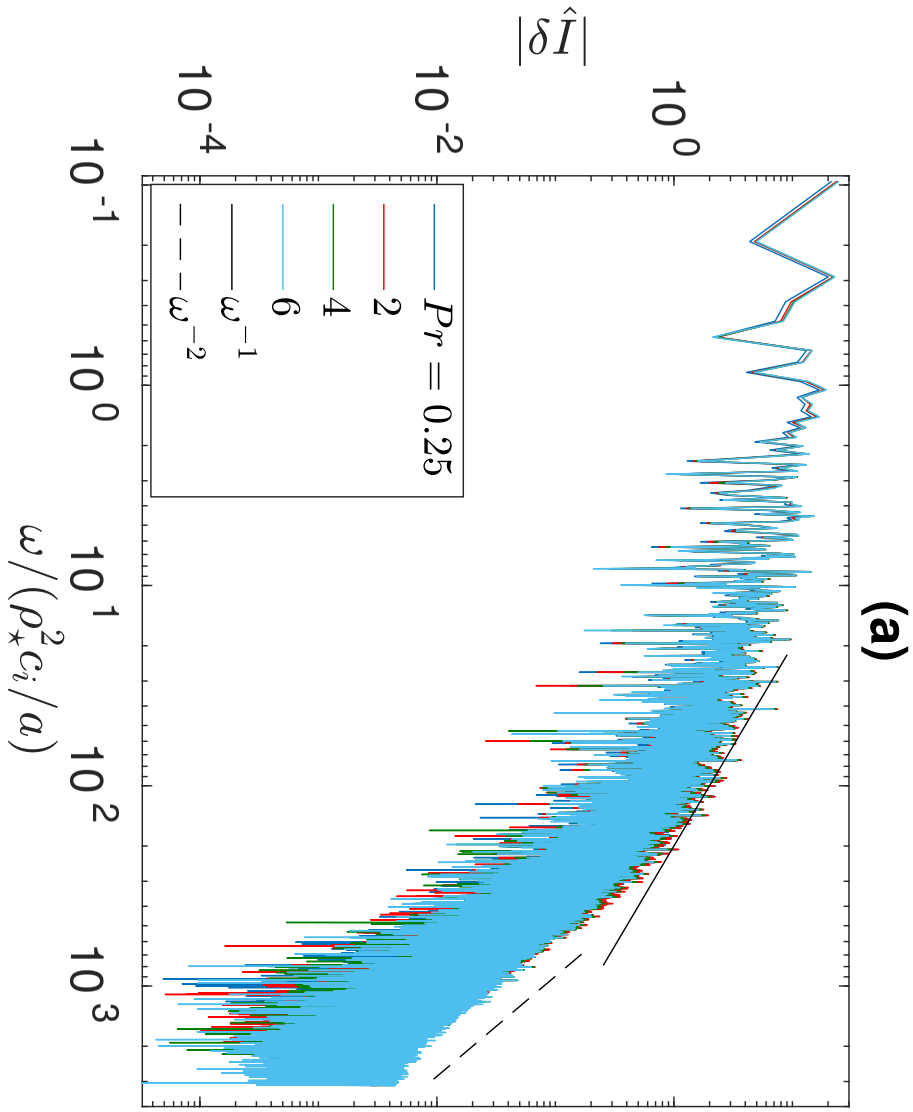

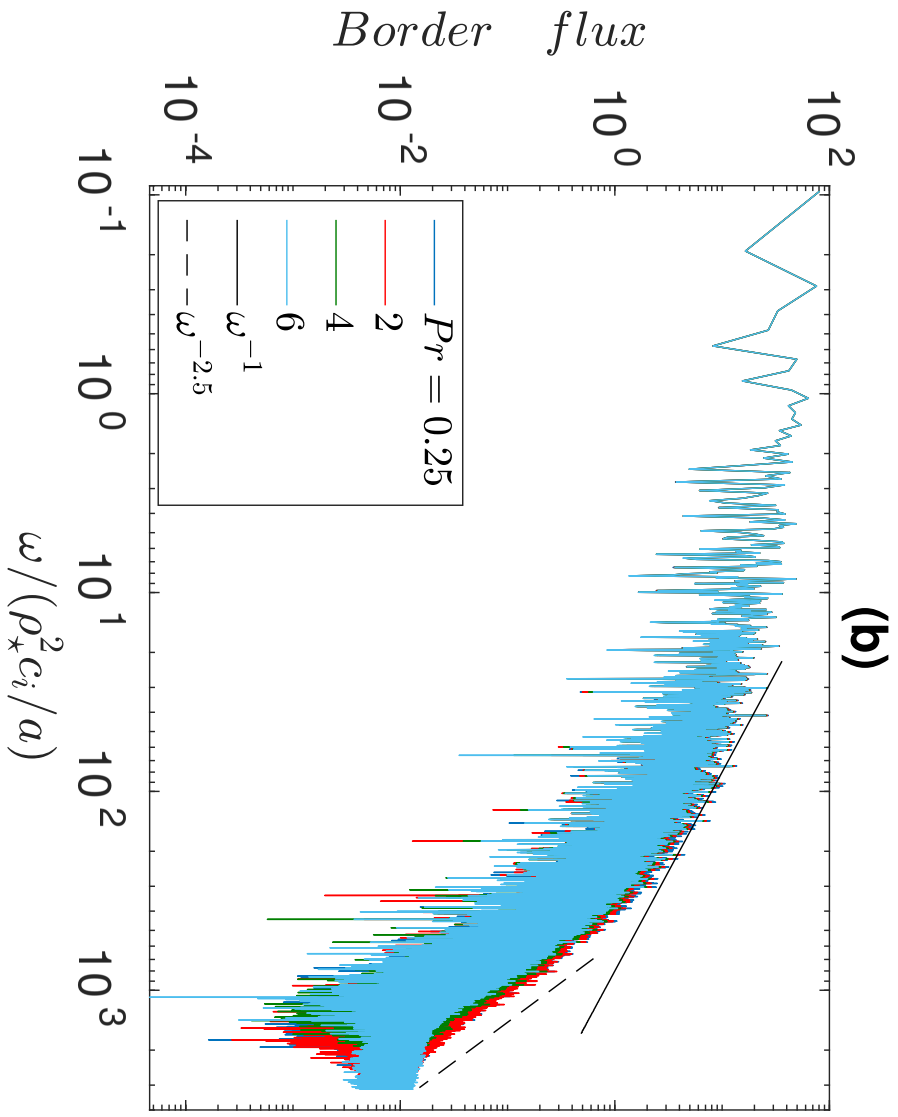

PLEASE CITE THIS ARTICLE AS DOI: 10.1063/1.5117835

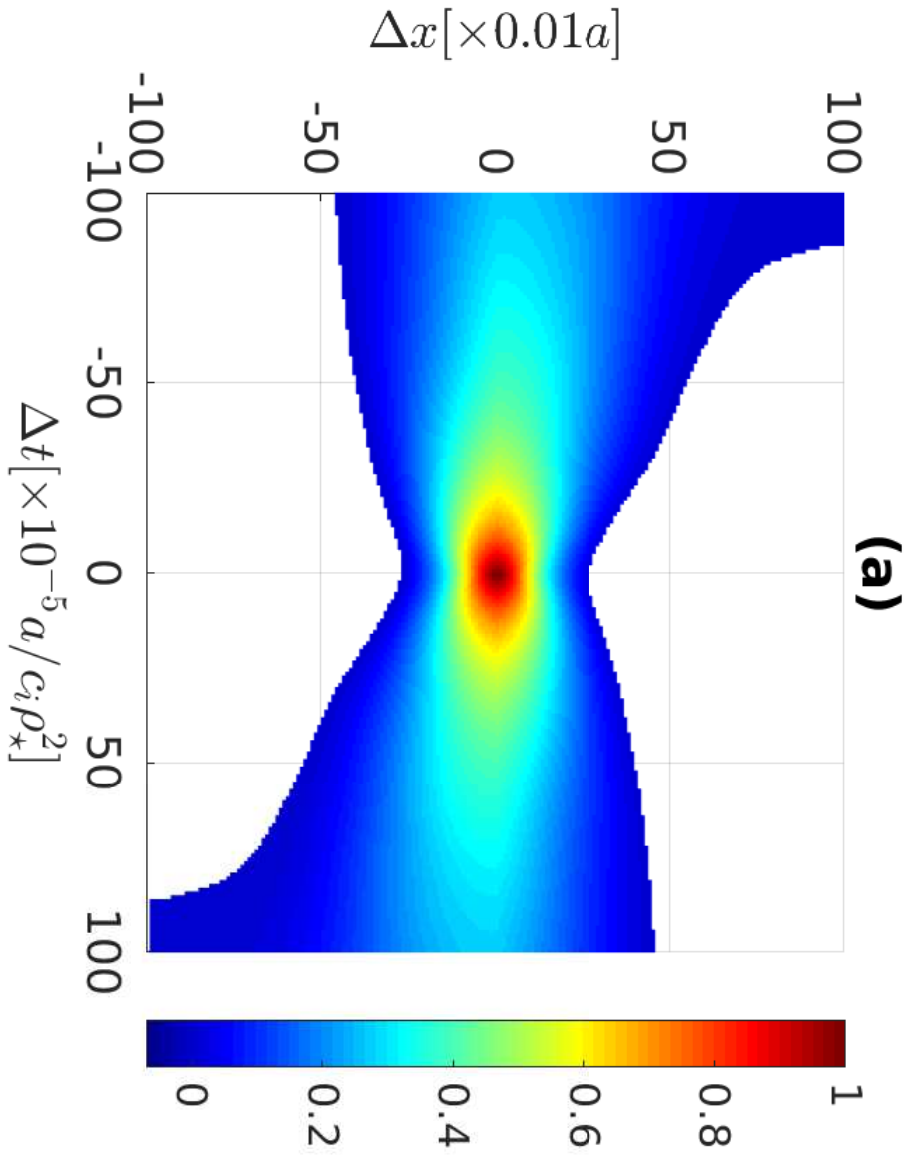

PLEASE CITE THIS ARTICLE AS DOI: 10.1063/1.5117835

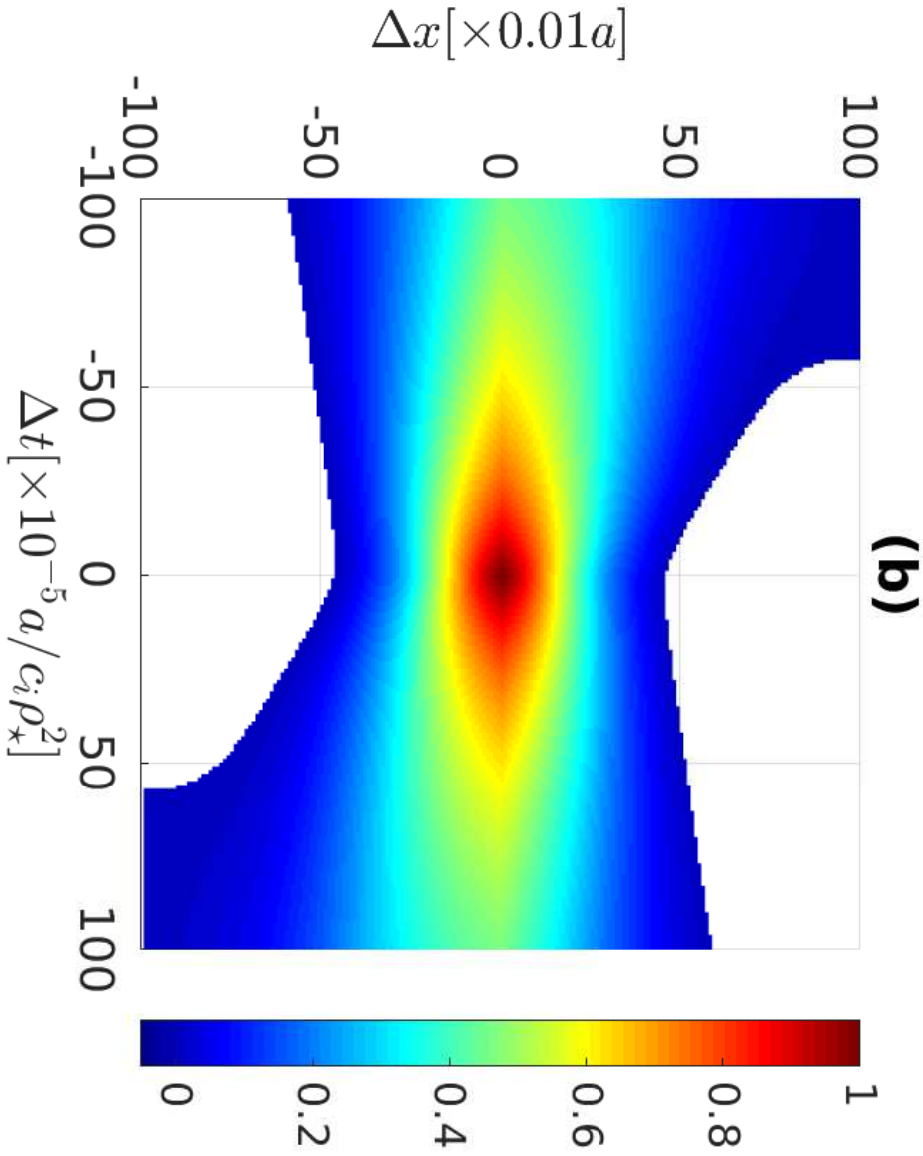

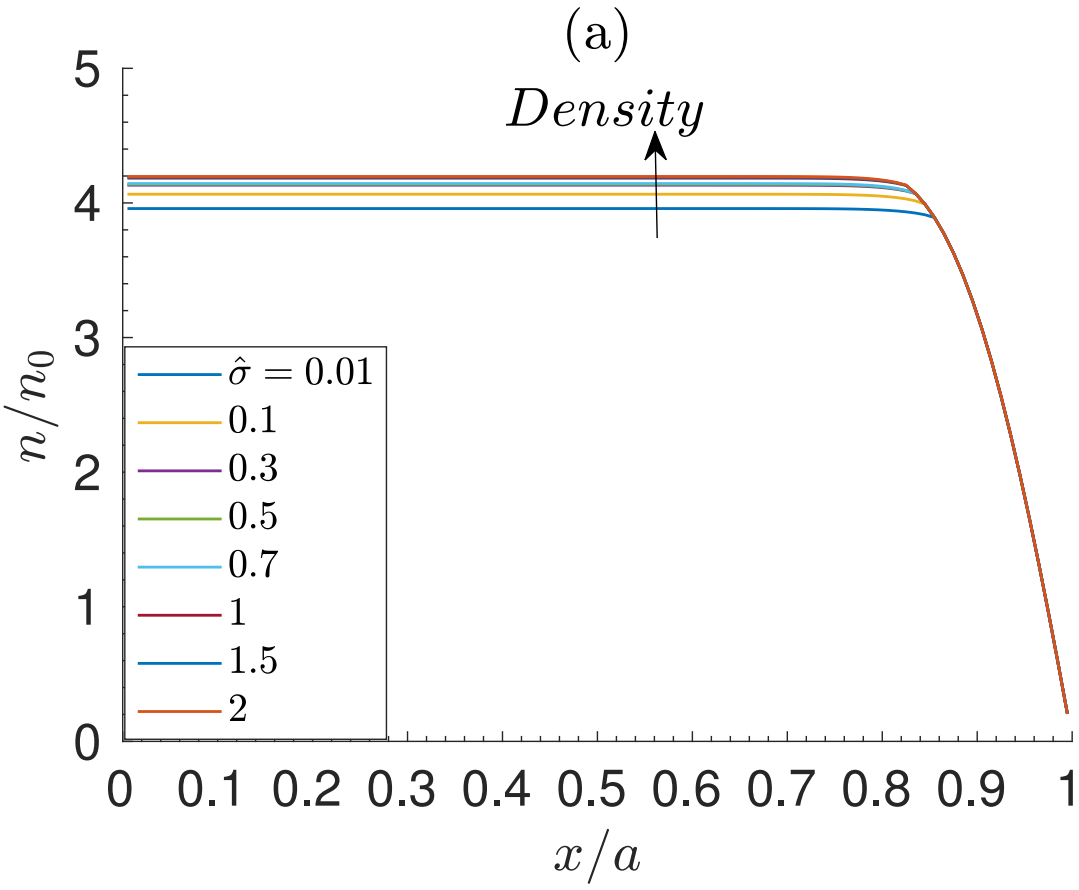

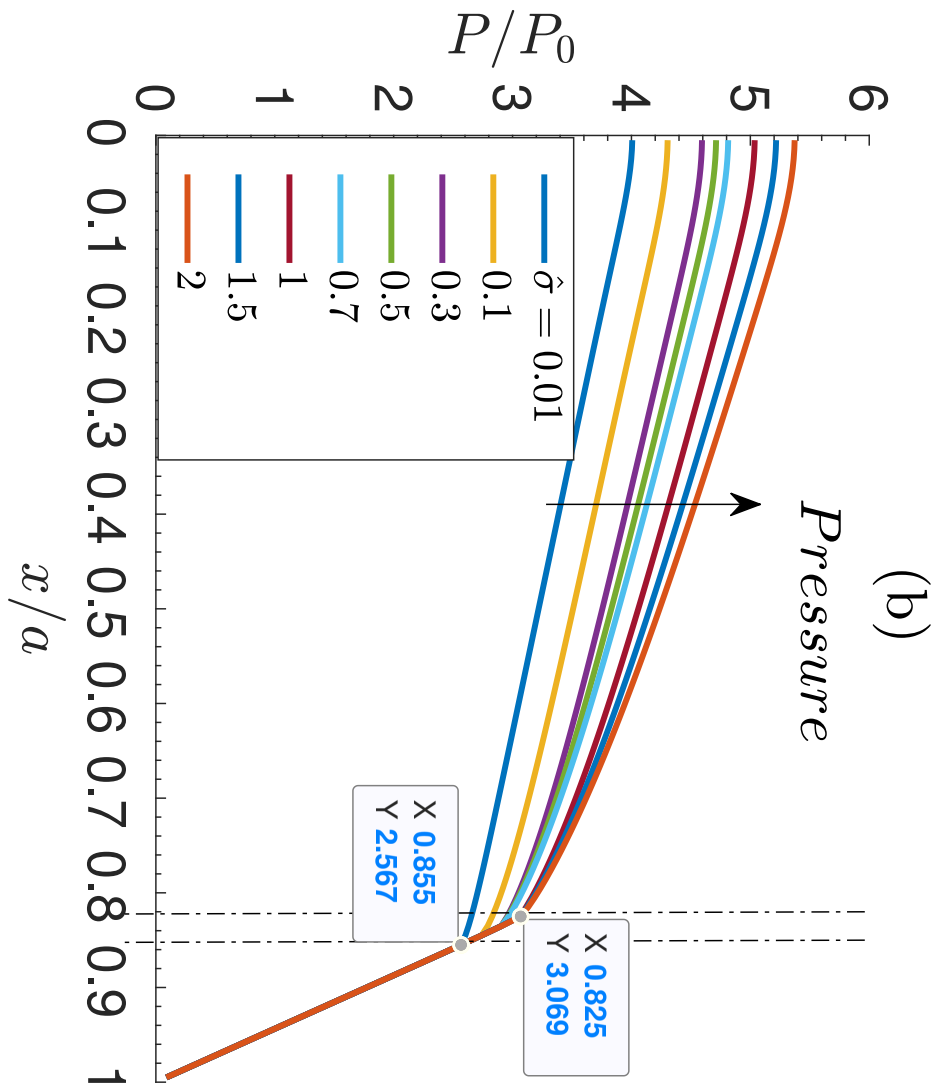

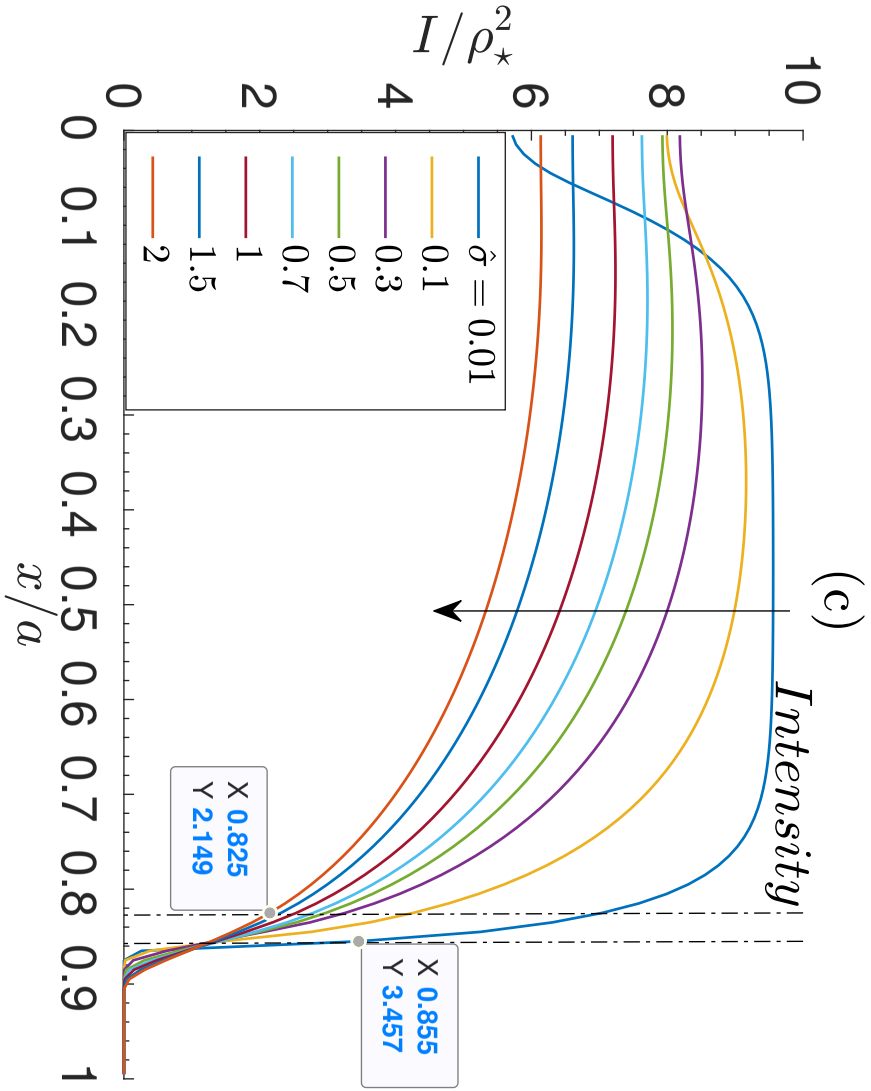

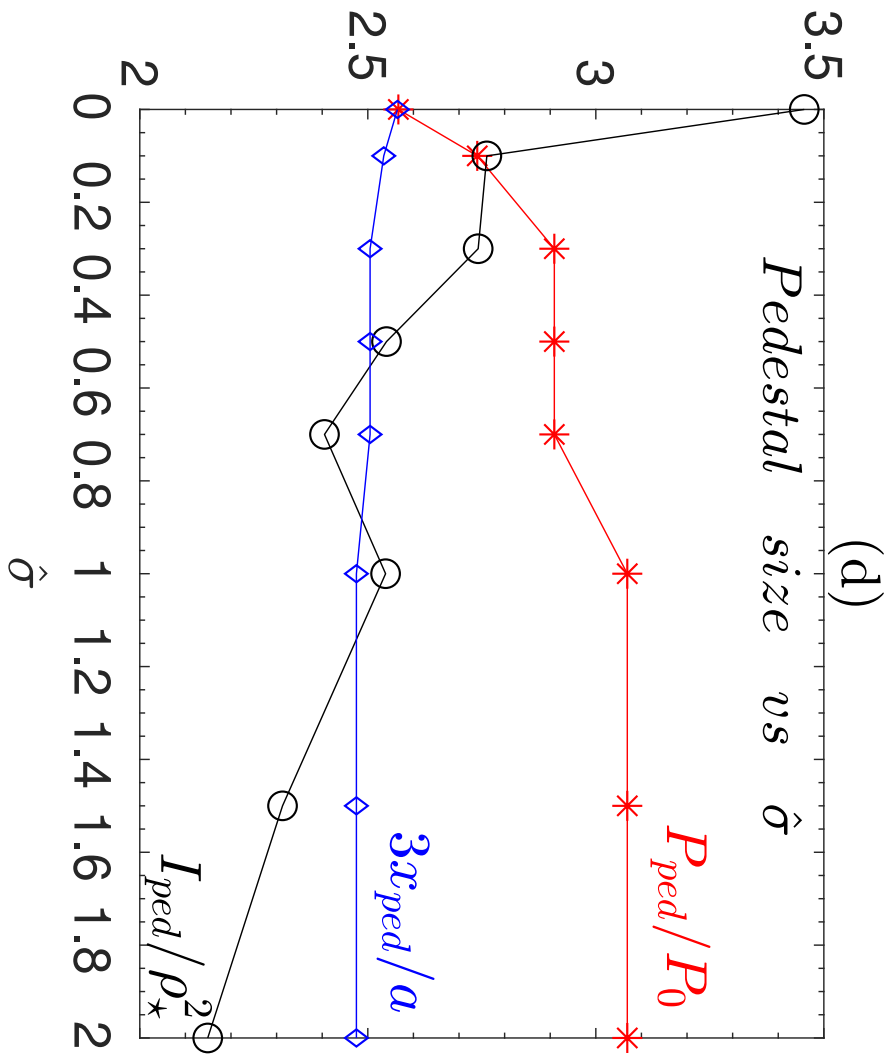

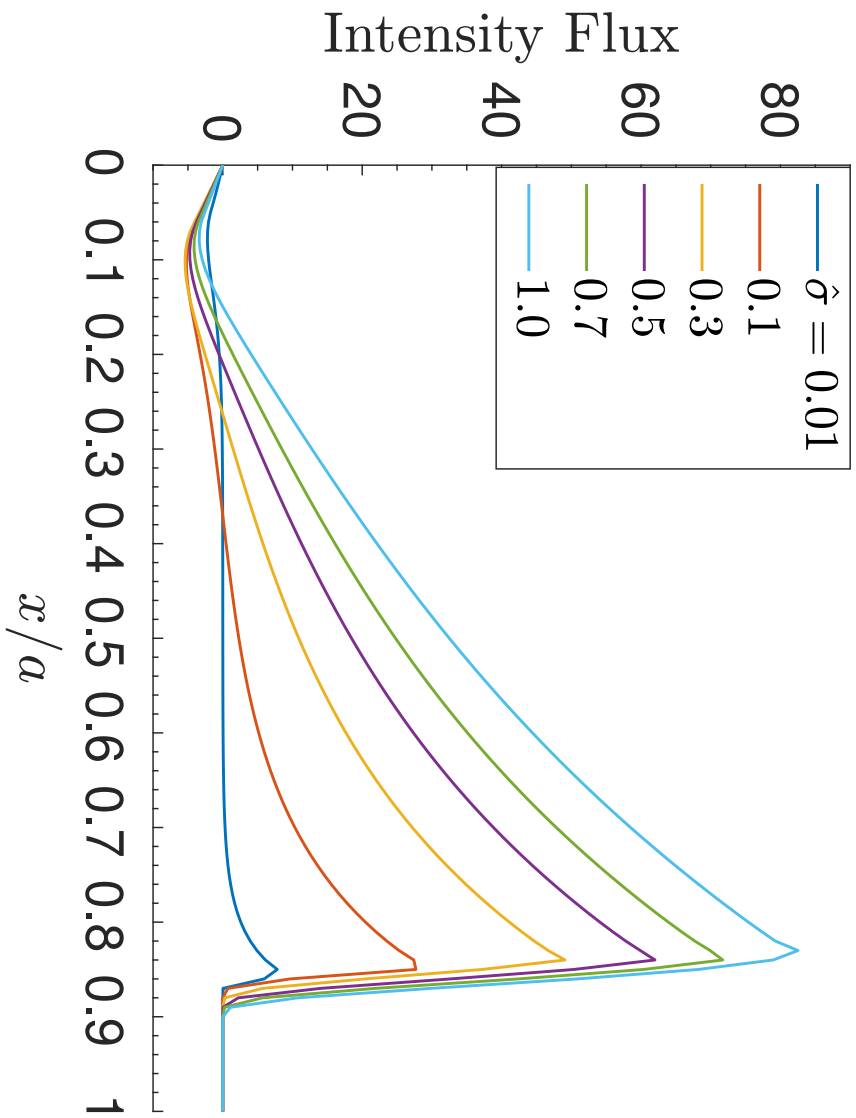

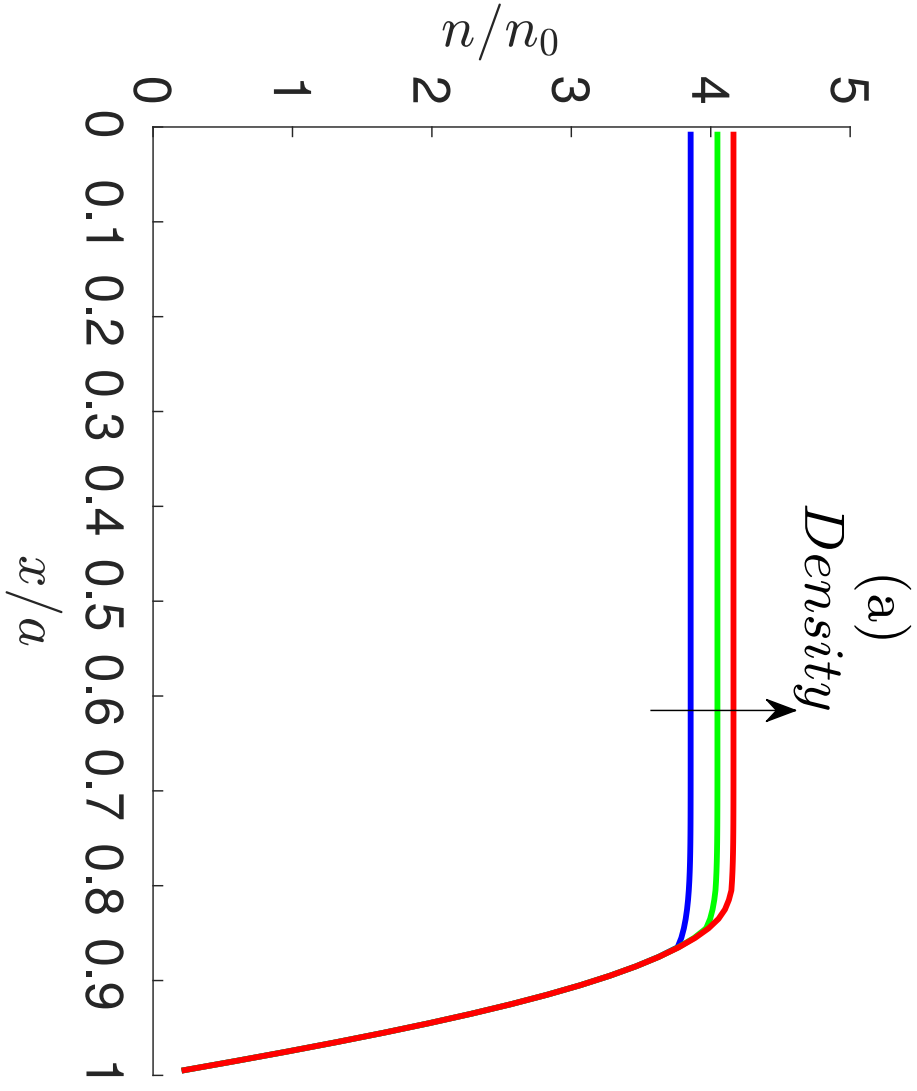

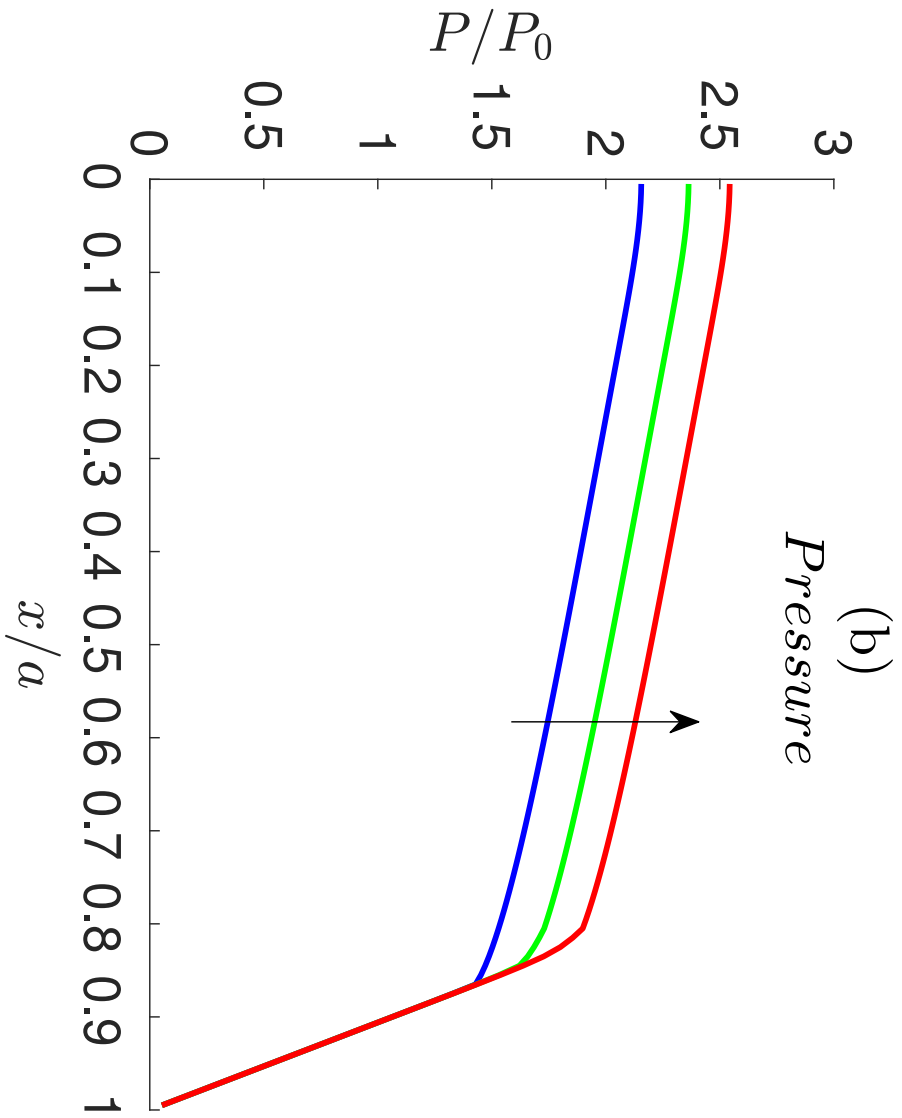

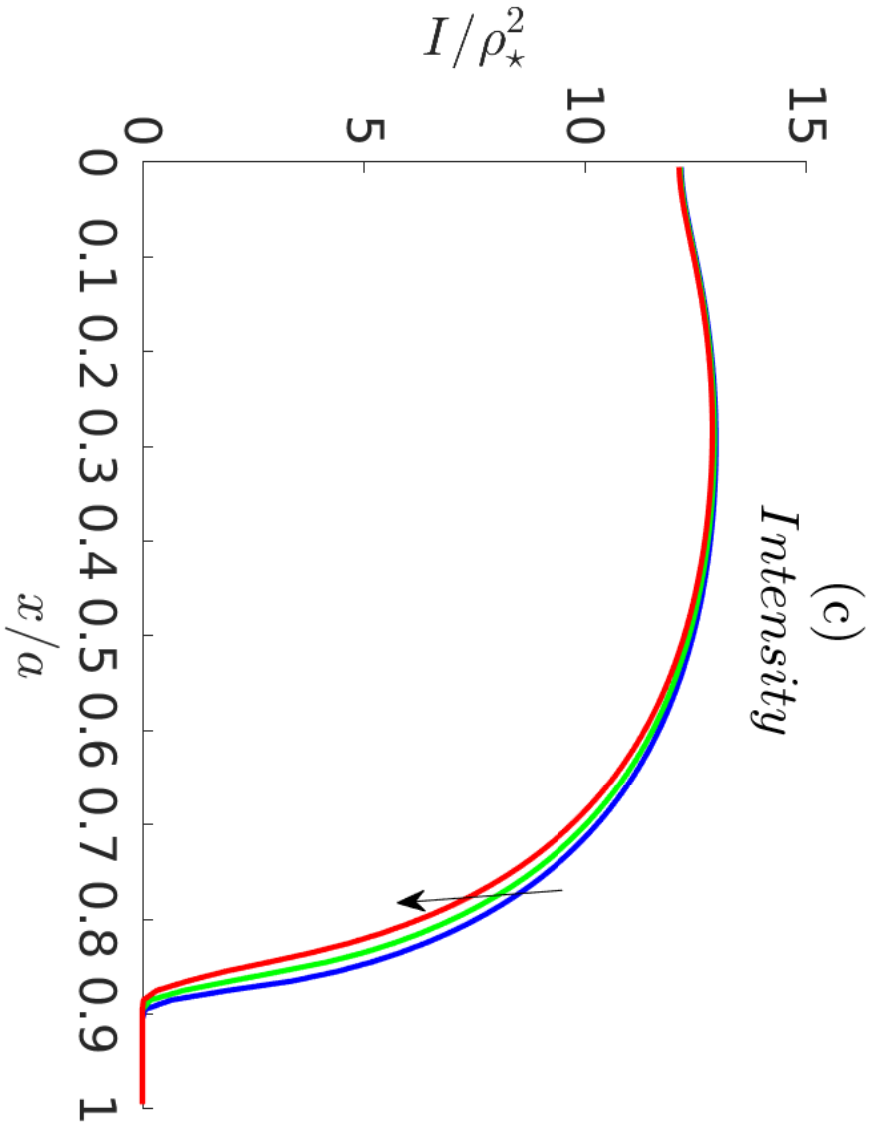

PLEASE CITE THIS ARTICLE AS DOI: 10.1063/1.5117835